





RESEARCH ARTICLE

10.1002/2017JC012868

Modeling North Atlantic Nor'easters With Modern Wave Forecast Models

Will Perrie¹ , Bechara Toulany¹, Aron Roland², Mathieu Dutour-Sikiric³, Changsheng Chen⁴ , Robert C. Beardsley⁵ , Jianhua Qi⁴ , Yongcun Hu¹, Michael P. Casey¹ , and Hui Shen¹

Key Points:

- Three modern wave forecast model systems are compared on fine-resolution grids for the Northwest Atlantic: WAVEWATCHIII (WW3), SWAN, SWAVE
- Three intense midlatitude storm cases: a spring Nor'easter in May 2005, the Patriots Day storm in 2007, and the Boxing Day storm in 2010
- Models that use advanced physics, like ST4, tuned to regional characteristics for the Northwest Atlantic can give enhanced results

Correspondence to:

W. Perrie,
William.Perrie@dfo-mpo.gc.ca

Citation:

Perrie, W., Toulany, B., Roland, A., Dutour-Sikiric, M., Chen, C., Beardsley, R. C., . . . Shen, H. (2018). Modeling North Atlantic Nor'easters with modern wave forecast models. *Journal of Geophysical Research: Oceans*, 123, 533–557. <https://doi.org/10.1002/2017JC012868>

Received 7 MAR 2017

Accepted 31 OCT 2017

Accepted article online 3 NOV 2017

Published online 24 JAN 2018

¹Fisheries & Oceans Canada, Bedford Institute of Oceanography, Dartmouth, NS, Canada, ²Institute for Hydraulic and Water Resources Engineering, Technische Universität Darmstadt, Darmstadt, Germany, ³Department of Marine and Environmental Research, Rudjer Boskovic Institute, Zagreb, Croatia, ⁴School for Marine Science and Technology, University of Massachusetts-Dartmouth, New Bedford, MA, USA, ⁵Department of Physical Oceanography, Woods Hole Oceanographic Institution, Woods Hole, MA, USA

Abstract Three state-of-the-art operational *wave forecast model systems* are implemented on fine-resolution grids for the Northwest Atlantic. These models are: (1) a composite model system consisting of SWAN implemented within WAVEWATCHIII[®] (the latter is hereafter, WW3) on a nested system of traditional structured grids, (2) an unstructured grid finite-volume wave model denoted “SWAVE,” using SWAN physics, and (3) an unstructured grid finite element wind wave model denoted as “WWM” (for “wind wave model”) which uses WW3 physics. Models are implemented on grid systems that include relatively large domains to capture the wave energy generated by the storms, as well as including fine-resolution nearshore regions of the southern Gulf of Maine with resolution on the scale of 25 m to simulate areas where inundation and coastal damage have occurred, due to the storms. Storm cases include three intense midlatitude cases: a spring Nor'easter storm in May 2005, the Patriot's Day storm in 2007, and the Boxing Day storm in 2010. Although these wave model systems have comparable overall properties in terms of their performance and skill, it is found that there are differences. Models that use more advanced physics, as presented in recent versions of WW3, tuned to regional characteristics, as in the Gulf of Maine and the Northwest Atlantic, can give enhanced results.

1. Introduction

This paper is part of an integrated network study that was launched by IOOS (USA Integrated Ocean Observing System) in 2010 entitled “The Super-Regional Testbed to Improve Models of Environmental Processes for the US Atlantic and Gulf of Mexico.” A related description is given by Chen et al. (2013). In particular, this part of the initiative was to evaluate the capabilities and limitations of the wave models used in *three* fully coupled wave-ocean model systems: (i) SWAN driven at lateral boundaries by WAVEWATCHIII[®] (the latter is hereafter, WW3) and coupled to ocean models, specifically ADCIRC; (ii) SWAVE coupled to FVCOM; and (iii) WWM coupled to SELFE, in simulations of coastal and oceanic sea states induced by three extratropical storms in the Gulf of Maine region. More details are given by Chen et al. (2013) for the ocean models ADCIRC, FVCOM, and SELFE. The focus for the *Super-Regional Testbed* network study was chosen to be Scituate Harbor, between Boston and Cape Cod. However, because no wave measurements are available in Scituate Harbor, the focus of this paper is *not* Scituate Harbor. Our focus in this paper is on the performance of the wave model systems, composed of the SWAN, WW3, SWAVE, and WWM wave models, in simulating the waves generated in the storm cases, *in uncoupled mode*, without influences from the respective ocean models. Model results are compared to measured wave data from buoys and satellite altimetry in the Northwest Atlantic, providing a detailed overview of model performance over the main development region for the storms considered in this study.

The simulation and forecasting of intense cyclones, including nor'easters and their ocean surface waves, are important issues, particularly with increased populations, human activities, and societal infrastructure, in coastal areas. These storms can generate rapidly changing winds that can create large complex storm-driven waves and storm surges that impact the shoreline when storms make landfall. These environmental processes are of concern to recreational users, marine transportation, fisheries, and offshore installations,

such as oil and gas resource developments. When storms make landfall, waves contribute to coastal damage and inundation. Low-lying coastal areas are vulnerable, such as the coastal areas of the southern Gulf of Maine. Historically, strong extratropical cyclones, e.g., nor'easters, have often been the drivers for coastal waves and storm surges in this area. An example is the Perfect Storm in October 1991, sometimes called the Halloween Storm, which generated maximum trough-to-crest elevations in excess of 30 m (Cardone et al., 1996; Donald Cameron and George Parkes, 1992). Associated wind gusts reached 33 m/s, with flooding from Cape Ann to Nantucket.

The third-generation spectral models used in this study are advanced: SWAN (Simulating WAVes Nearshore) version 40.81, and WW3 version 4.18. SWAN was developed for high-resolution coastal and nearshore applications; whereas WW3 is suitable for global, regional basin-scale, shelf-scale, and coastal studies, and has also been used for nearshore shallow water applications, with numerical and physical parameterizations for these spatial scales. SWAN was developed by Booij et al. (1999), with updates described by the SWAN Team (2013, available at <http://swanmodel.sourceforge.net/>). WW3 was developed at NCEP and is described by Tolman and WAVEWATCH III Development Group (2014) and Tolman (2002, 2008, 2009). We use two formulations of SWAN and WW3. As used here, SWAN refers to the standard *structured* (traditional regular longitude-latitude) grid version of Booij et al. (1999). SWAVE is an *unstructured* finite-volume wave model, which was developed by converting the SWAN code under the platform of FVCOM (Qi et al., 2009). For WW3, we use the standard version implemented on nested *structured* mosaic grids described by Tolman and WAVEWATCH III Development Group (2014), and also, an *unstructured* grid finite-element version, denoted WWM (wind wave model), described by Roland (2009) and Roland et al. (2012).

In this study, these wave models are implemented in *three wave model systems*:

1. *Structured* hierarchical grids with SWAN implemented on three inner—nested *structured* high-resolution grids, within two outer—nested two-way coupled coarser grids where WW3 is used,
2. SWAVE implemented on a set of nested finite-volume *unstructured* grid domains, and
3. WWM implemented on a single finite-element *unstructured* grid.

These three *wave model systems* have the basic similarity that they all solve the wave action balance equation and use a selection of available standard source terms for wind input S_{in} (e.g., Janssen, 1991; Snyder et al., 1981), wave dissipation S_{ds} (e.g., Ardhuin et al., 2010; Komen et al., 1984), and nonlinear quadruplet interactions, S_{nl} (Hasselmann, 1960; 1962). SWAVE and SWAN include the same formulations for wave effects due to finite depth: wave dissipation, bottom friction, triad and quadruplet wave-wave interactions, and shallow water wave-breaking. WW3 and WWM use the same set of formulations for source terms S_{in} , S_{ds} and S_{nl} ; however, the numerics are *different*. WW3 uses a third-order upwind propagation scheme (Tolman and WAVEWATCH III Development Group 2014), whereas WWM uses lower-order propagation schemes (Roland et al., 2012). SWAN uses a fully implicit first-order scheme. SWAVE uses a second-order upwind scheme.

To evaluate the performance of these differing wave model systems, they are implemented on meshes that are approximately equivalent, in terms of their resolutions and their coverage of the essential areas needed to investigate waves generated during the storms' life cycles. For any given storm, we use the *same* wind fields to drive the waves. Three storms are considered: a Nor'easter Storm from May 2005, the Patriot's Day Storm in 2007, and the Boxing Day Storm in 2010. Model validation is based on wave data from buoys and satellite altimeters. Section 2 presents an overview of the wave model systems and their setups. Section 3 describes the storm cases. Section 4 presents the simulation results. A discussion of the results is presented in section 5, followed by conclusions in section 6. The plan of this study is to: (i) *conduct comparisons of model systems with the same physics (different numerics)*, (ii) *conduct comparisons of specific models with different physics*, (iii) *investigate the results of model tuning* to reflect the regional characteristics of the focus area of this study, e.g., the Gulf of Maine and the Northwest Atlantic. It is well known that WW3 is tuned to optimize forecast skill for the Global Ocean and needs to be (slightly) recalibrated for specific local regions, such as the focus area of this study.

2. Wave Models

The wave model system composed of WW3 and SWAN was implemented on five nested computational domains. WW3 was implemented over the two outermost grid domains (Figures 1a and 1b), using its

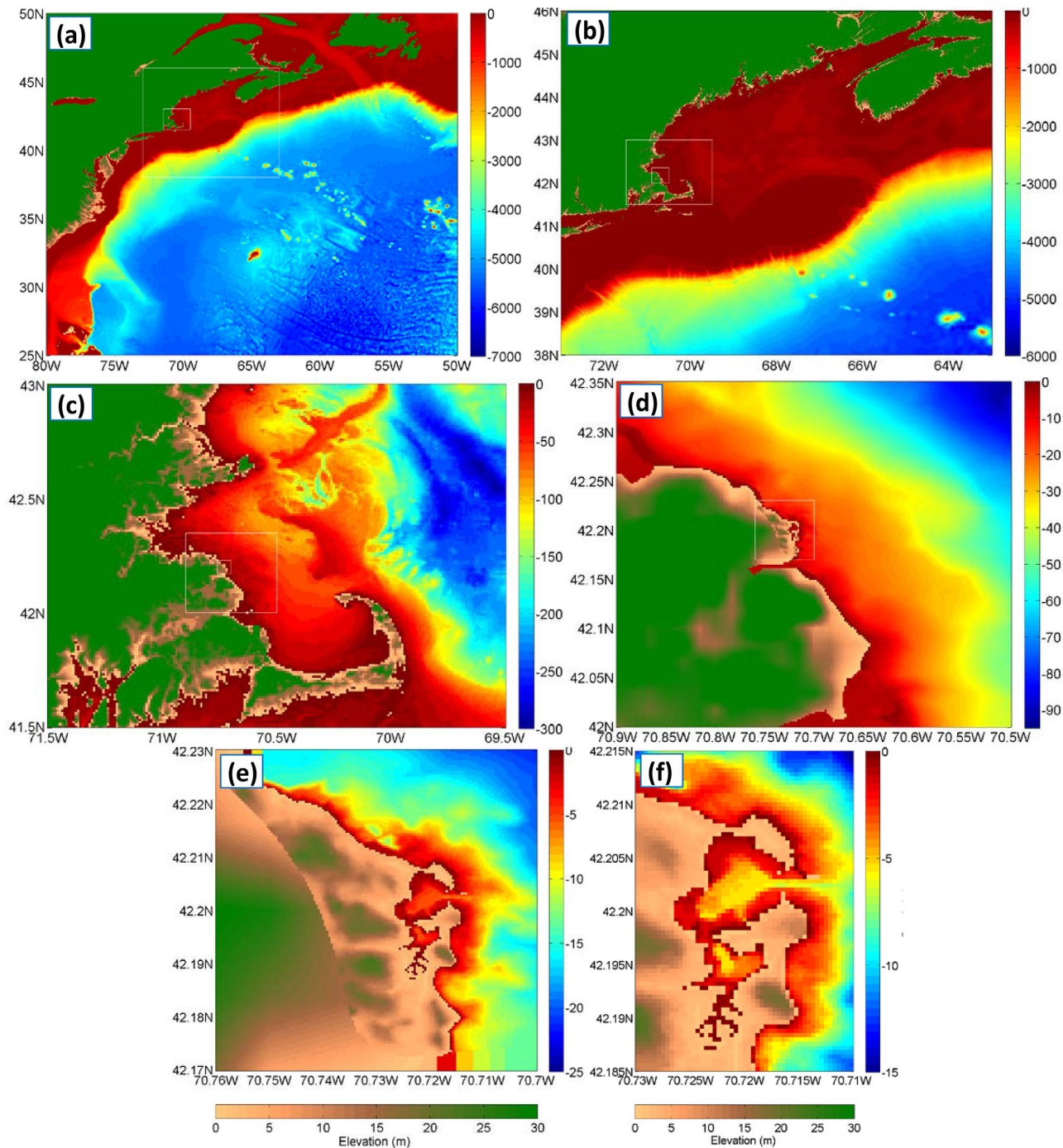


Figure 1. Integration grids used by the three wave models, showing BIO structured nested grid system; SWAN for inner three grids, WW3, outer two grids, with bathymetry and elevation are indicated (m), for: (a) grid 1 at 1/5° resolution, (b) grid 2 at 1/20° resolution, (c) grid 3 at 1/100° resolution, (d) grid 4 at 1/500° resolution, (e) grid 5 at 1/2500° resolution, and (f) a zoom view of Scituate Harbor from grid 5.

mosaic multigrid, with two-way nesting between the grids. SWAN was implemented for the three innermost nested grids (Figures 1c–1e).

In terms of physics, WW3 uses the present *operational* state-of-the-art physics for S_{in} and S_{ds} following Ardhuin et al. (2010), hereafter denoted ST4, in comparison with baseline physics, which is the original formulation for S_{in} and S_{ds} of the WAMDI Group (1988), denoted ST1, in conjunction with JONSWAP-type bottom friction (Hasselmann et al., 1973; Tolman, 2002), depth-induced wave breaking (Battjes & Janssen, 1978) and

the so-called third-order ultimate-quickest propagation scheme. Simulations include the older relatively simplistic ST1 parameterizations because ST1 constitutes the physics formulations that were available to SWAN and SWAVE, at the time of the study. In comparisons presented here, WWM also uses ST1 and ST4 formulations to represent S_{in} and S_{ds} . The nonlinear quadruplet wave-wave interactions (S_{nl}) are parameterized by DIA—the discrete interaction approximation (Hasselmann et al., 1985; WAMDI Group, 1988), as used in most operational forecast wave models. More advanced ST4 physics has a cost; a 24 h. simulation on the two outermost grids in Figure 1 takes 200 s using WW3 with ST1 physics with 32 CPUs on a cluster computer at Bedford Institute of Oceanography, whereas the time is 316 sec using ST4 physics.

In the WW3-SWAN formulation, WW3 and SWAN output 2-D wave spectra at boundary points of each outer grid, which are used as boundary conditions to drive the nested wave model implemented in the next inner-nested domain. The same methodology is used in the SWAVE implementation, which has multiple nested *unstructured* grid domains; 2-D wave spectra at each grid point on the outer boundary are passed to the next inner-grid point, to make the nesting of the domains. This is not a concern for WWM which has a single large multiscale unstructured grid.

For WW3-SWAN *structured* implementations for domains in Figures 1a and 1b, WW3 has 21 frequency bins, with lowest frequency 0.05 Hz, and an increment factor of 1.122018 on a logarithmically spaced grid. There were 36 directions, with $\Delta\theta = 10^\circ$. For the outermost, coarsest resolution (~ 19 km) grid domain (Figure 1a), the maximum global time step is 600 s, whereas in the second nested grid domain (resolution 5 km) the maximum global time step of 120 s, satisfying the CFL criterion. SWAN was implemented for the three innermost grids (Figures 1c–1e), with the same frequency and directional discretizations as WW3. For the three innermost grids, SWAN resolutions were 1 km, 190 m, and ~ 38 m, with time steps of 300, 60, and 60 s, respectively, representing $12 \times$ the CFL criterion using SWAN's implicit scheme. SWAN uses ST1 physics for S_{in} and S_{ds} , with bottom friction (Collins, 1972), depth-induced wave breaking (Battjes & Janssen, 1978), and refraction. Triad wave-wave interactions were not used in this study.

SWAVE also uses ST1 physics for S_{in} and S_{ds} and the *same* frequency and directional discretizations and resolutions as SWAN. The *unstructured* grid is given in Figure 2a, nested within a larger regular grid where the boundary conditions are provided by WW3 (using either ST1 or ST4 depending on the test case) with a resolution of ~ 10 km, as implemented by Chen et al. (2013). The governing equations for SWAVE are solved using second-order, flux-based discrete finite-volume methods, described by Qi et al. (2009). Time integration uses a semi-implicit integration scheme as used in the WAM model (WAMDI Group, 1988) and WW3 (Tolman, 2002). The horizontal grid resolution (measured along the longest edge of a triangular cell) varies from 0.3 to 1.0 km in the coastal region and up to 10 km near the outer boundary. Mean water depths at all nodes are taken from the USGS 15 arcsec digital bathymetry data set, with a minimum depth of 3 m at the coast. A maximum depth cutoff of 1,500 m is imposed in the slope region south of the shelf break. The regional grid implementation of the SWAVE domain in Figure 2a is much smaller than those of the other two models.

WWM uses a hybrid fractional step method, where the geographical advection is solved using implicit residual distribution schemes (Roland, 2009) and spectral space is integrated the same way as done in the WW3 model. The source terms are integrated semi-implicitly within the advection scheme. WWM uses an unstructured grid with a large outer domain, compared to implementations for WW3-SWAN and SWAVE (Figure 2b). A triangular spatial grid is constructed, with a refined mesh in the southern Gulf of Maine and 20 m edge length resolution in nearshore waters of Scituate Harbor. For consistency with the other models, WWM uses 21 discrete frequencies, from 0.05 to 0.5 Hz and 36 directional bins. In terms of physics, WWM uses either ST1 or ST4, (Roland, 2009; Roland et al., 2012). In other studies, WWM has been coupled to ocean circulations models such as SELFE and ROMS (Dutour Sikiric et al., 2012; Roland et al., 2012). Here, in this study, our focus is on the performance of the wave model systems in simulating the waves generated in the storms, *in uncoupled mode*, without influences from the circulation models.

In terms of propagation schemes and integration methodologies, WWM uses implicit first-order schemes and the integration scheme for the source terms is based on Patankar (1980) allowing a larger time step (for WWM, 600 s). This kind of integration scheme for the source terms is also used by SWAN. This implies that the source term limiter also applies to the spatial propagation part and is therefore expected to act more strongly on wave growth and dissipation processes in SWAN and WWM than in the dynamic integration

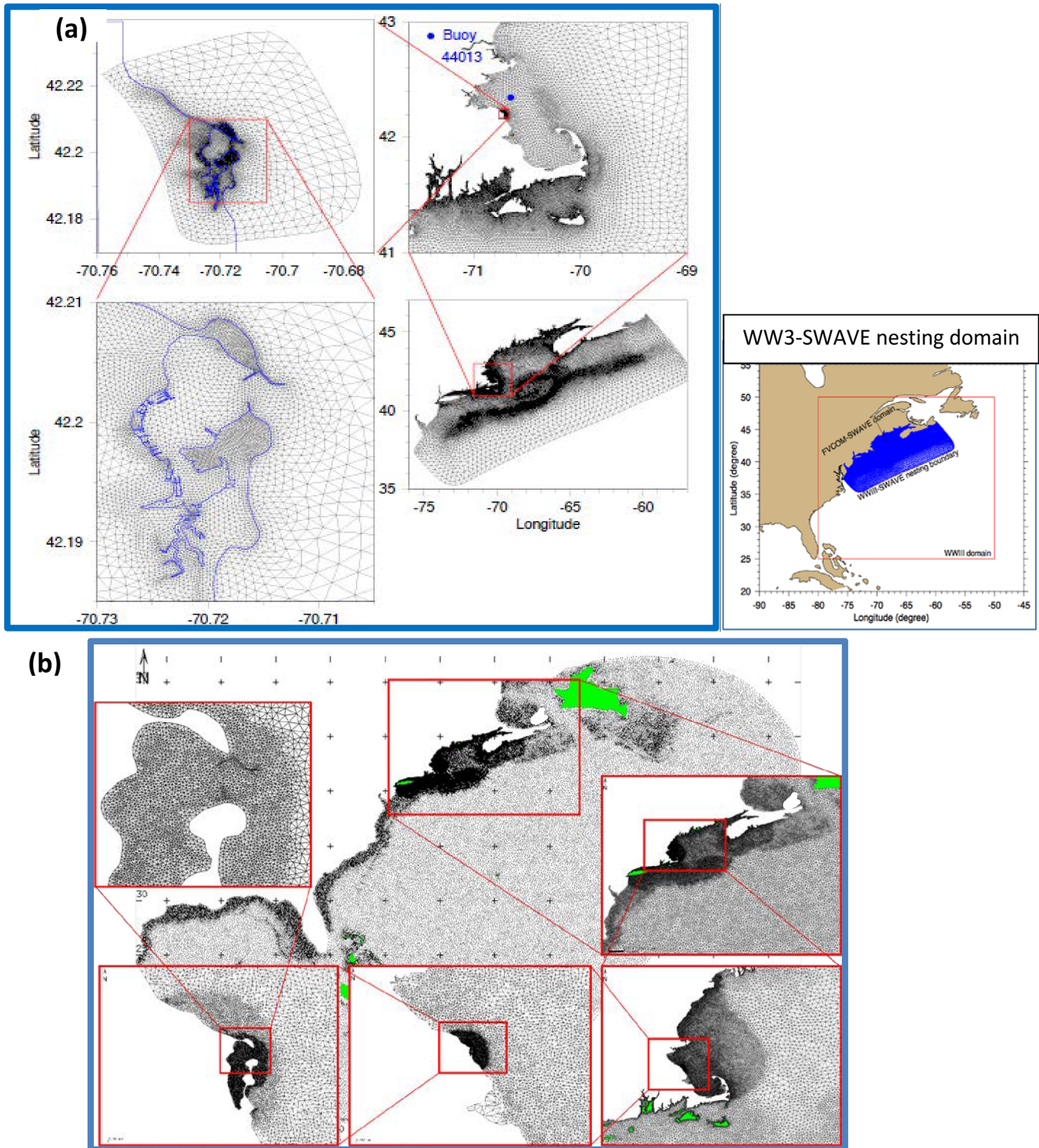


Figure 2. (a) University of Massachusetts unstructured triangular grid of the SWAVE model showing Scituate harbor area, (top left) nested within regional grid (bottom right), (top right) with a zoomed view of the Massachusetts coast bounded by the red box in the regional grid. Blue dot is location of NDBC 44013. (bottom left) Zoomed view of Scituate Harbor bounded by the red box shown in the (top left) regional grid. (b) Numerical mesh, from top to bottom, focusing on Scituate Harbor as used in the WWMIII implementation and model simulations.

scheme of WW3, where a specified number of time steps are allowed before the limiter is used to constrain the solution. Higher-order schemes are not used in WWM in this study because of their strongly dispersive characteristics, their limitations in terms of the multiscale grid, e.g., from very deep ocean areas to very high-resolution nearshore areas, and related time-step dependencies of convergent solutions.

Boundary conditions at the outermost boundary for each model system are assumed to behave like a solid wall; nothing comes in and the boundary is like a sponge which absorbs all waves crossing to the outside. However, as the swell field in the North Atlantic is about 1 m on average, assuming no waves on the outermost boundary implies that there could possibly be 1 m bias in the simulated H_s estimates in these model systems. Furthermore, the nonlinear wave-wave interactions which are simulated by the DIA (Discrete Interaction Approximation) in the wave model systems depend on the swell field. Thus, the missing part of the swell spectra energy may affect the nonlinear interactions (S_{nl}) as well. However, no boundary effect is evident in the storms considered in this study, as shown in the observed buoy data (below, Figure 10); no low-frequency swell is evident.

The notation for model results reported in this paper is given here. Results from the model system using WW3 with ST1, ST4, and ST4 m (a modified form of ST4 described in section 4a below) physics, nested to SWAN, are denoted simply as WW3-ST1, WW3-ST4, and WW3-ST4m, respectively, rather than written as “WW3-SWAN-ST1,” etc., throughout the manuscript. In all these simulations, SWAN uses only the basic ST1 physics. This is to simplify notation. When WAVEWATCHIII is used just by itself, we denote this as WW3 and we explicitly state what source terms are used. Results from WWM with ST1 and ST4 are denoted WWM-ST1 and WWM-ST4, respectively. Results from SWAVE with ST1 (the only option available) are denoted simply as SWAVE.

3. Storm Cases

Each year, tropical storms and nor'easters passing northward along the New England coast have the potential to cause coastal inundation, major damage to infrastructure, and loss of life. Nor'easters typically form between October and April when cold dry continental air meets warmer moist marine air along the south-east U.S. coast, intensifying as they propagate to the northeast along the coast. They can intensify explosively, developing hurricane-strength winds.

3.1. 2005 Nor'easter Storm

Late in the day on 5 May 2005, a surface low formed over Florida as a 500 hPa trough and began to deepen, subsequently moving northeast along the coast. Early on 6 May, the system began to deepen rapidly. Over North Carolina surface pressures began to plummet ahead of the low, and coastal winds began to increase significantly. The low continued to deepen rapidly as it crossed south of Cape Hatteras. At 2000Z, the low center was estimated at 995 hPa located at 50 miles SSE from buoy 41025 which reported NNE winds at 40 kts gusting to 58 kts. As the system continued to move northeast out into the North Atlantic on 7 May, convection began wrapping around the center of circulation and a distinct eye feature persisted. The system developed strong convection at its circulation center as its location moved along the northern edge of the Gulf Stream, an area with strong SST gradients and continued toward the northeast.

3.2. Patriot's Day Storm 2007

An area of low pressure intensified rapidly as it moved slowly from the southeastern U.S. on the morning of Sunday, 15 April, to near New York City by Monday, 16 April 2007. The intense low over New York City, in combination with high pressure over eastern Canada, produced a high pressure gradient across the area, resulting in strong east-to-northeast winds. The storm caused widespread power outages, knocked down trees, and caused closure of numerous roads near the coast. Strong winds produced a storm surge and maximum waves of more than 10 m. A combination of storm surge, large waves, and high tides resulted in coastal flooding and erosion, particularly in areas of the southern Gulf of Maine. Subsequently the Patriot's Day Storm drifted slowly eastward over a 5 day period and gradually weakened.

3.3. Boxing Day Storm 2010

This was a classic nor'easter. It started as a large extratropical low pressure system off North Carolina on 26 December, strengthening to a gale as it approached Cape Cod and southeastern Massachusetts the next day. In tracking over the Mid-Atlantic Bight, it had a drop in pressure of about 20 hPa, by almost 1 hPa/h. Winds and waves measured at NDBC buoys 44013 and 44008 (Figures 3 and 4) show the passage of this storm. The

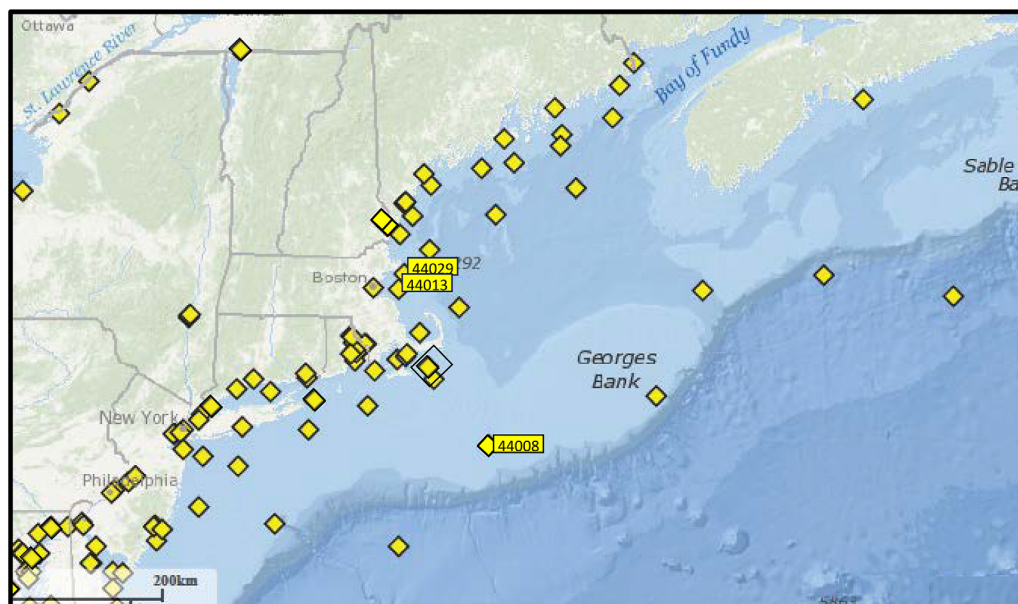


Figure 3. Location of NDBC (National Data Buoy Center) buoys and other observations in the Northeast Atlantic, with 44013, 44029, and 44008 highlighted in yellow. From NDBC website.

storm arrived at buoy 44008 at about 02 UTC 26 December, when winds from the northeast started to increase, eventually reaching a peak of ~22 m/s. Sea level pressure at Scituate dropped from 1013 hPa at 09 UTC 26 December to 971 hPa at 06 UTC the next day, 42 hPa in 21 h. The pressure drop at buoy 44013 constructed by Chen et al. (2013) using MM5 was similar, but lagged Scituate by about 5 h. As the storm passed Scituate (about 8 UTC), the winds shifted to the northwest (offshore in Massachusetts Bay) and decreased over the next 24 h. Waves at buoy 44013 increased to about 8 m by ~10 UTC, then rapidly subsided.

3.4. Wind Fields

The surface winds used to drive the wave models were derived from hindcasts made with the Northeast Coastal Ocean Forecast System (NECOFS) for the Gulf of Maine. Specifically, the *model* winds used in this study were constructed by Chen et al. (2013) using MM5 (Grell et al., 1995; <http://www2.mmm.ucar.edu/mm5/>) for the 2005 storm and WRF (Powers et al., 2017; <http://www2.mmm.ucar.edu/wrf/users/>) model simulations for the 2007 and 2010 storms, blended with NARR (North American Regional Reanalysis) winds (Mesinger et al., 2006) for outer parts of the wave model domains, to cover the large wave model grid domains, e.g., shown in Figure 2. The MM5 and WRF models were driven by the North American Meso-scale (NAM) Weather Model. The MM5 and WRF models started with the NAM 27 × 27 km forecast and produced the 9 × 9 km forecast hourly winds used in this study. For each model simulation, wind fields were interpolated bilinearly in time and space to the wave model grids.

To estimate the reliability of the *model* winds, they are also compared to time series wind data from NDBC (National Data Buoy Center) buoys (located in Figure 3) as well as the reanalysis fields from NARR and NCEP Climate Forecast System Reanalysis data (CFSR; Saha et al., 2010). NARR and CFSR winds have spatial resolutions of 32 km, and in time, 3 hourly. Results for buoys 44008, 44013, and 44029 are shown in Figure 4. This shows that the *model* winds achieve better comparisons to the buoy winds than results from either NARR or CFSR, during the three storms. The CFSR winds exhibit notable phase lags compared to the observed buoy winds in the Nor'easter Storm and the Patriot's Day Storm.

In terms of area distributions, we show area comparisons in Figure 5 for the main storm geographical areas at the peaks of each of the three storms. The *modeled* winds appear to be more similar to CFSR winds than to NARR winds. By contrast, NARR winds appear to have notable biases in central portions of each storm. Additional large-scale comparisons can be made with collocated remotely sensed altimeter measurements (Jason-1, Jason-2, ENVISAT, and ERS-2; Queffeuilou and Croiz-Fillon 2017). With respect to altimeter data and large-scale domains, Figure 6 suggests that the *model* winds and results from CFSR and NARR winds are

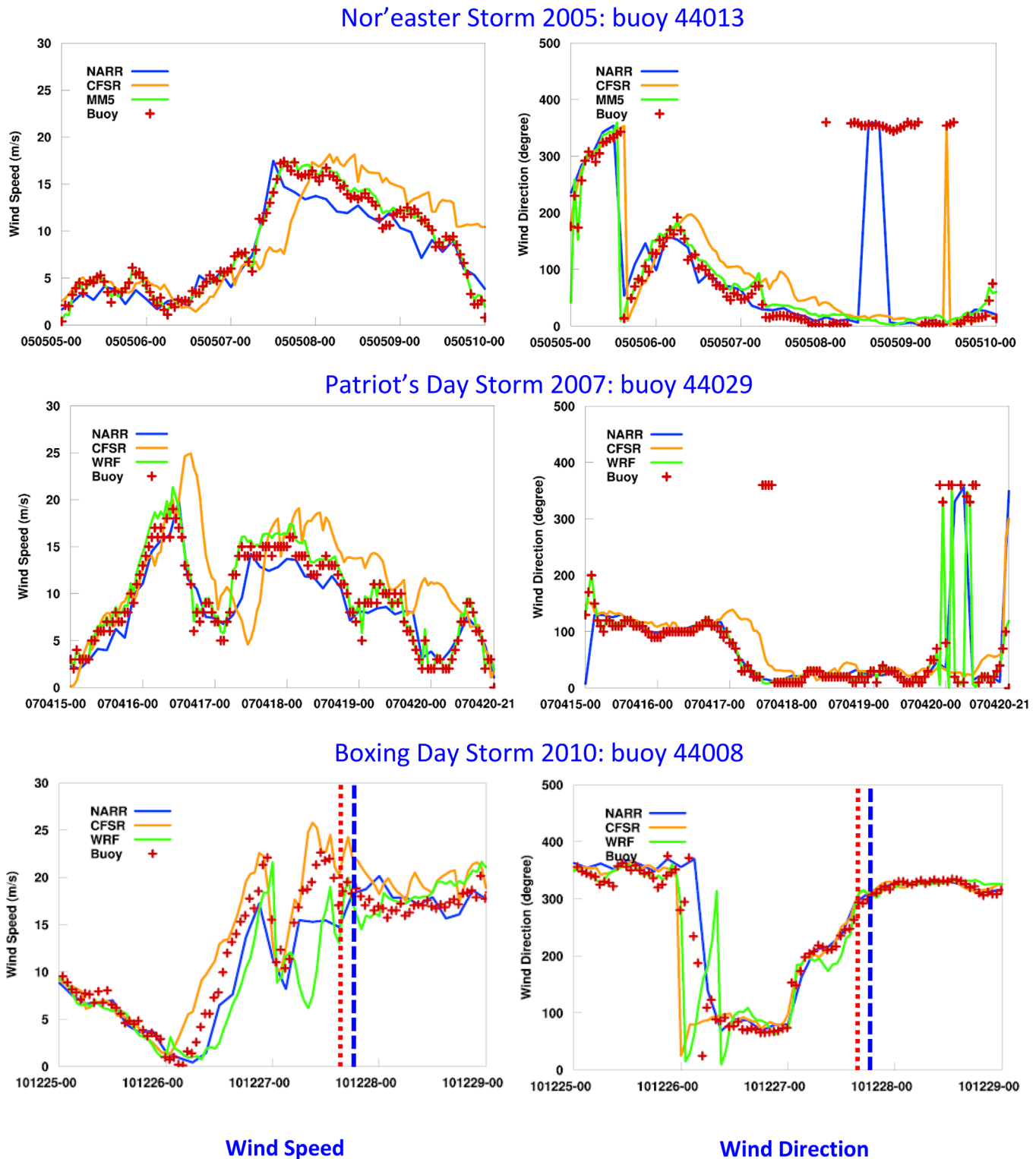


Figure 4. Time series comparisons, for observed wind speeds (m/s) and directions at buoys 44013, 44029, and 44008 during the 2005 (top row) Nor'easter Storm, (middle row) Patriot's Day Storm, and (bottom row) Boxing Day Storm, comparing NARR, CFSR, MM5, or WRF, to buoy measurements. Vertical lines indicate 15 UTC () and 18 UTC () on 27 December during the Boxing Day Storm, for comparisons in Figure 11 below.

similar. With respect to the altimeter wind data, the correlation coefficients and root mean square errors (RMS) are, respectively, (0.82, 2.5), (0.83, 1.9), and (0.83, 2.4) for modeled winds, CFSR and NARR. In this comparison, the altimeter measurements come from a larger domain (80°–50°W, 25°–50°N) than the study area,

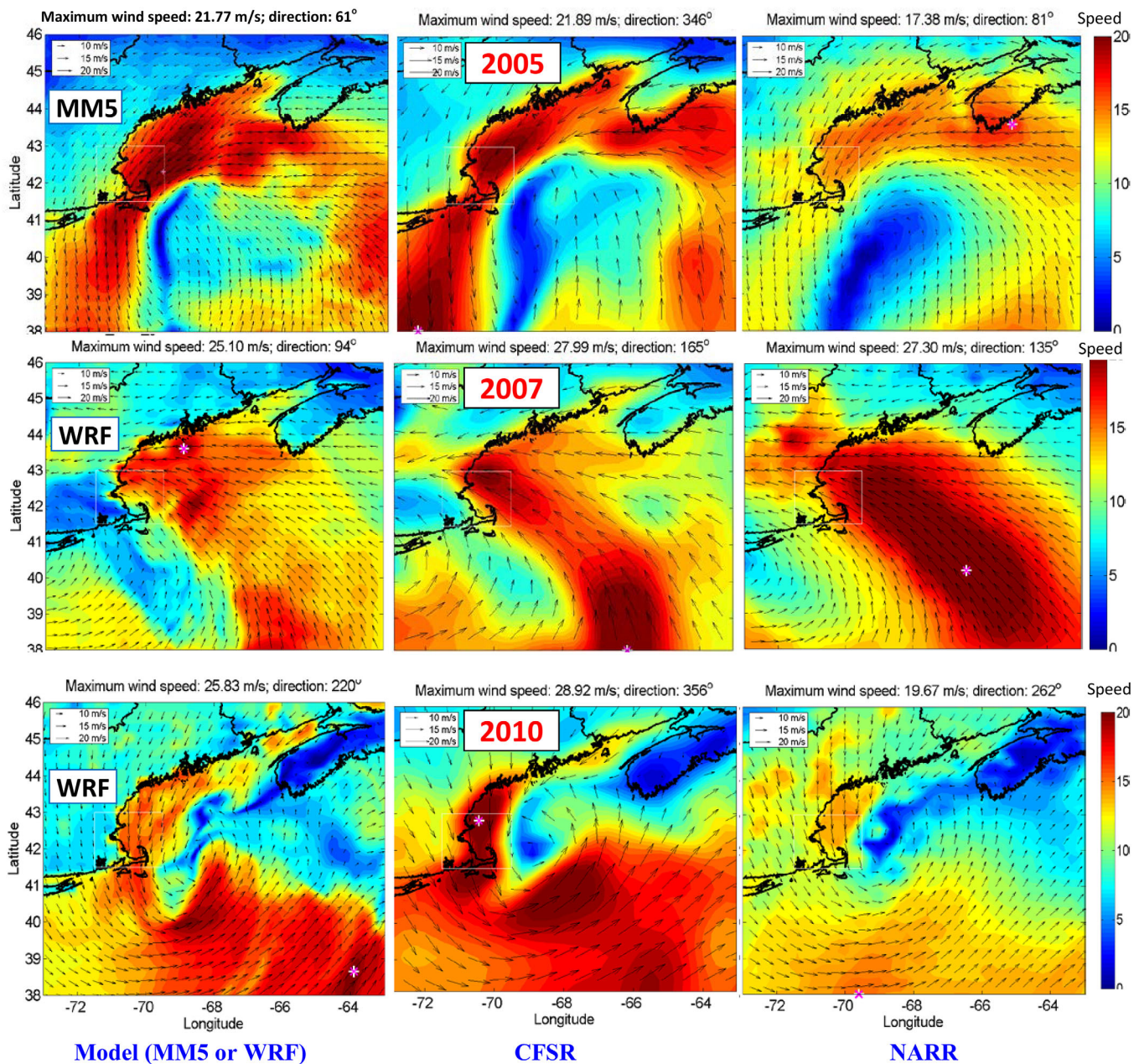


Figure 5. Area maps showing distributions of winds during three storms, 2005 Nor'easter Storm at 18UTC on (top row) 7 May, (middle row) Patriot's Day Storm at 12UTC on 16 April and (bottom row) Boxing Day Storm at 15UTC on 27 December, at the storm peaks, comparing the modeled winds (first column from left), CFSR winds (second column) and NARR winds (third column). Units are m/s as indicated by the color bar.

which is the focus of this paper (72°–64°W, 38°–46°N). Thus, errors in the MM5/WRF winds blended with NARR winds, relative to altimeter data, are dominated by the NARR errors in the outer domain and error statistics of MM5/WRF—NARR blended data (0.82, 2.5) are very close to those of NARR data (0.83, 2.4). The selection of MM5/WRF forcing winds is based on their better agreement with buoy observations as shown in Figure 4.

4. Comparisons of Wave Model Results

4.1. Significant Wave Heights

Comparisons between time series of buoy measurements of significant wave heights H_s and the model estimates were made for the three storms. Figure 7 shows H_s time series at buoy 44013 near Scituate

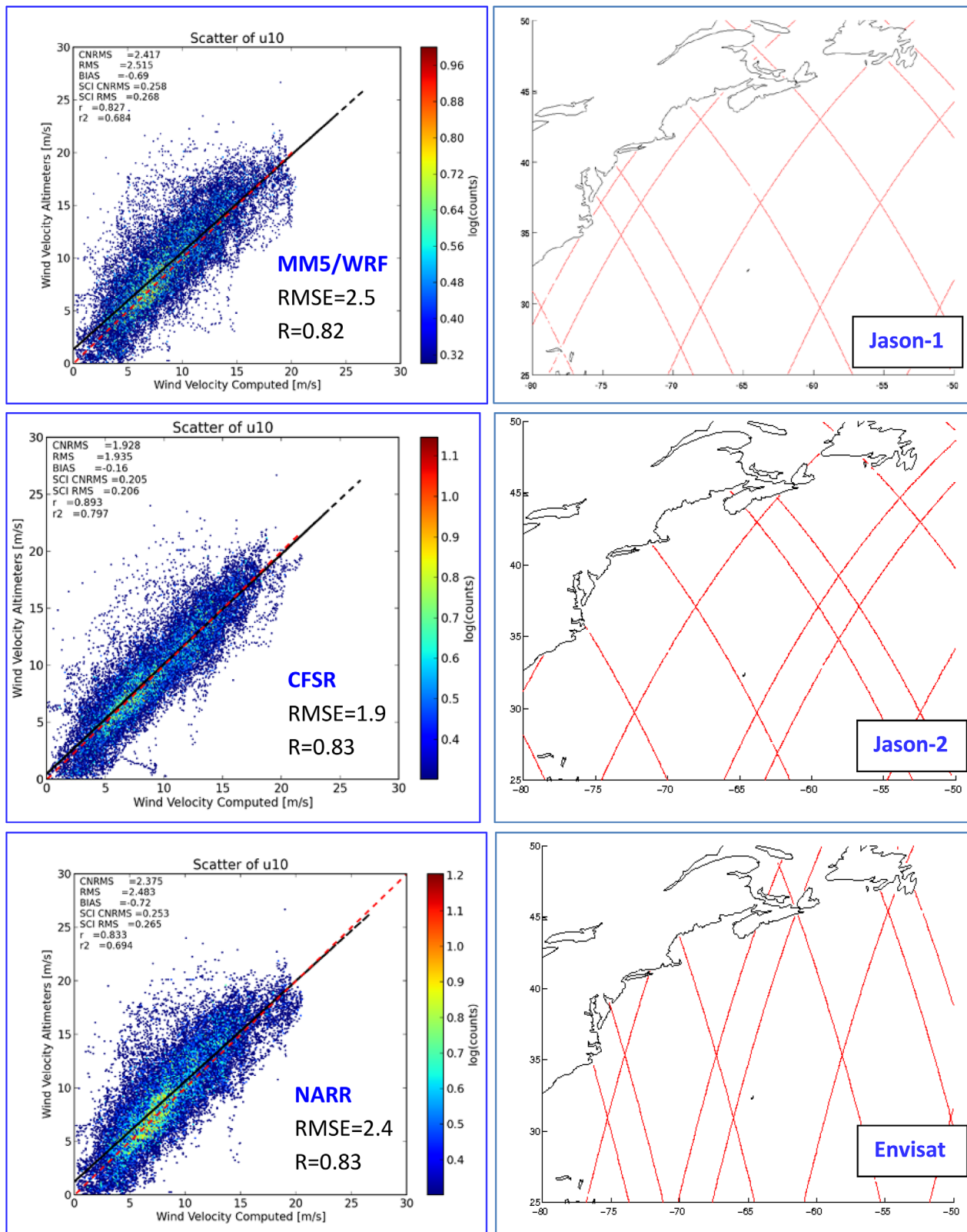


Figure 6. (left column, from top to bottom) Comparison of NARR blended with MM5 (2005 Noreaster Storm) or WRF (Patriots Day Storm), CFSR and NARR winds with all flying altimeters for the storm events in 2005 and 2007. (right column) Example tracks of altimeter satellites providing data; not shown is ERS-2, also used.

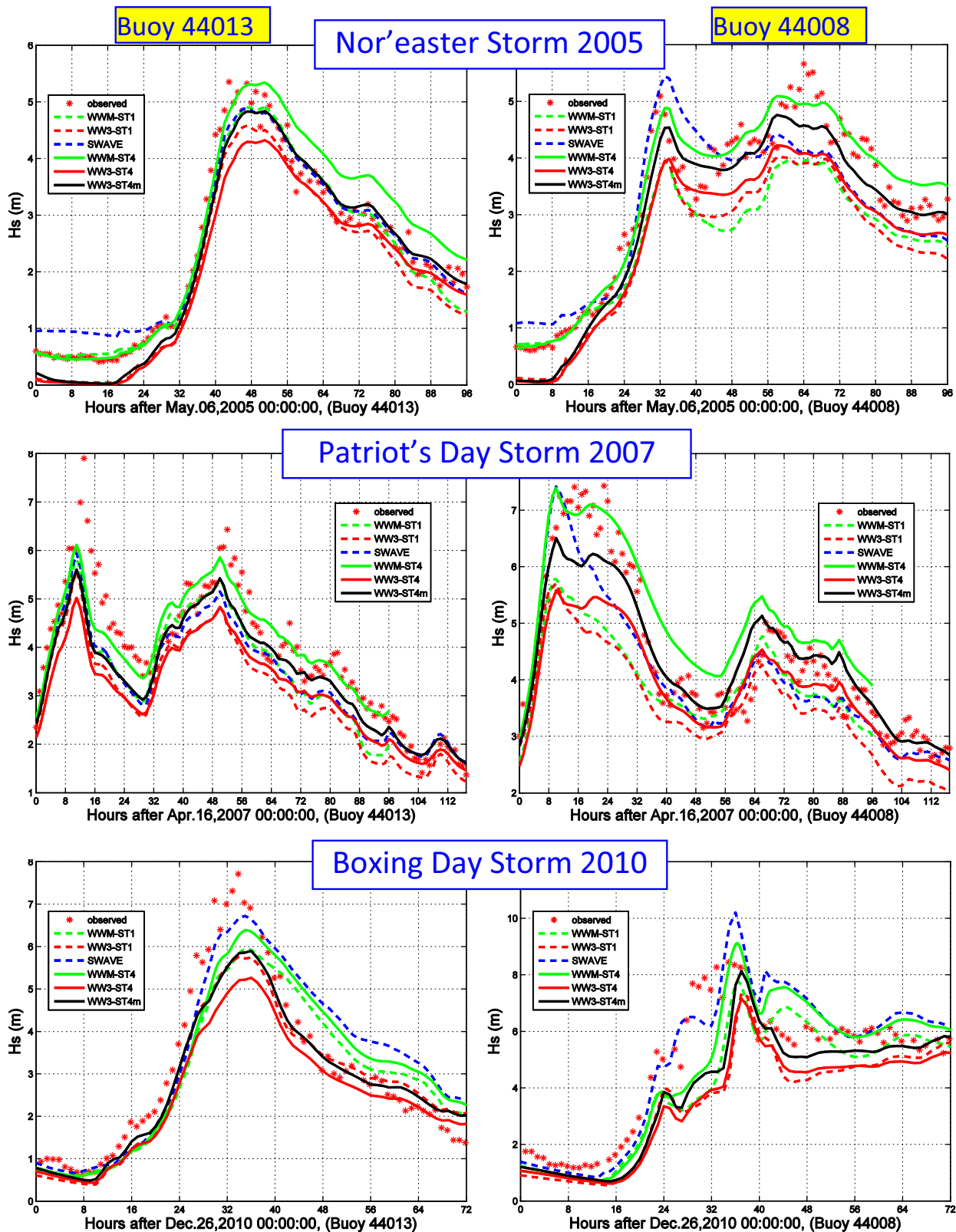


Figure 7. Time series comparisons for significant wave height H_s , for the three storms: (top row) 2005 Nor'easter Storm, (middle row) 2007 Patriot's Day Storm, and (bottom row) 2010 Boxing Day Storm. Results are shown at buoys 44013 (left column) and 44008 (right column), comparing buoy observations with wave models results, including ST1, ST4, and ST4m.

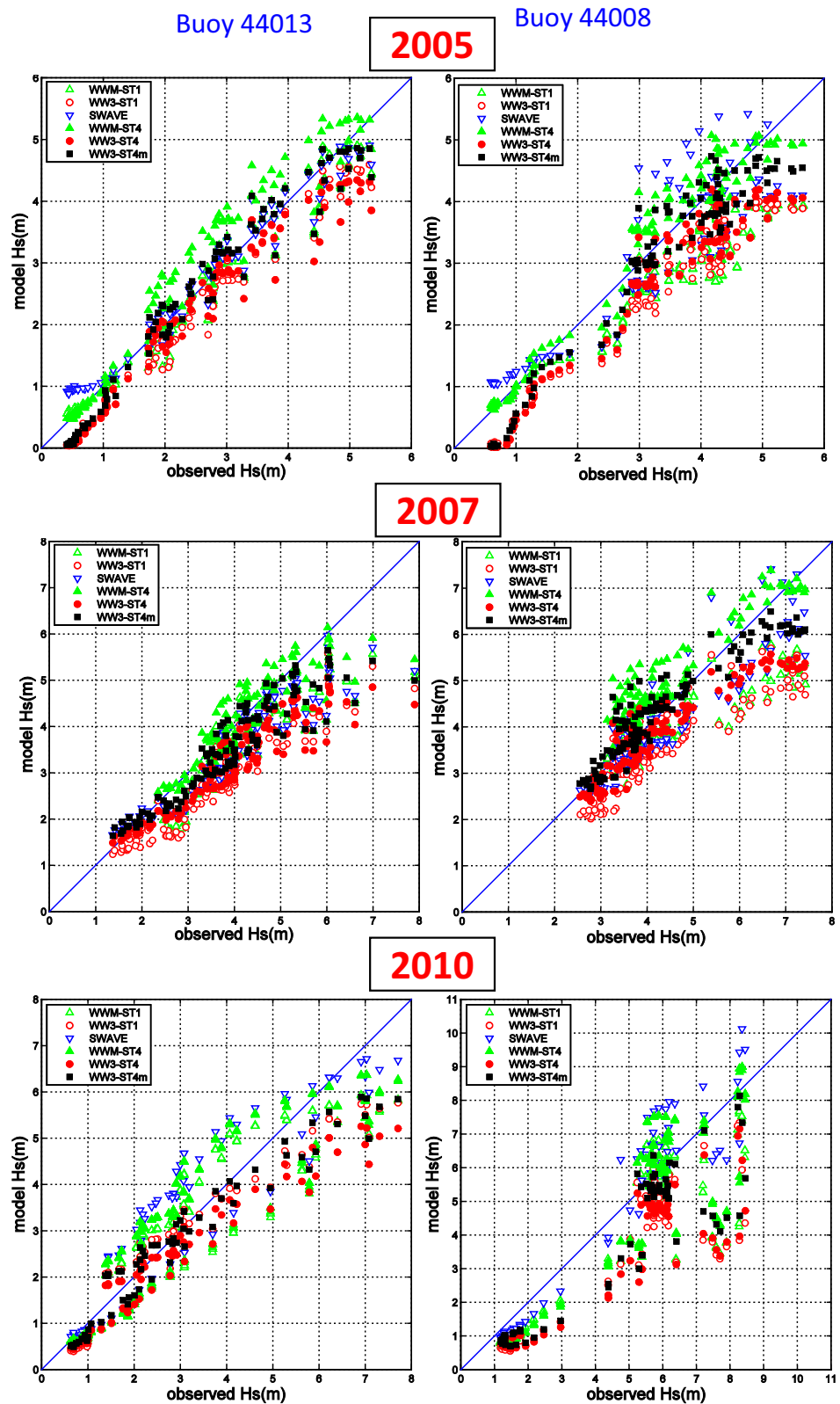


Figure 8. As in Figure 7, showing scatterplots for the three storms: (top) 2005 Nor'easter Storm, (middle) 2007 Patriot's Day Storm, and (bottom) 2010 Boxing Day Storm, at buoys 40013 (left column) and 44008 (right column), comparing buoy observations with wave models results, including ST1, ST4, and ST4m. See Tables 1 and 2 for statistical results.

Table 1
 Statistics for $H_s(m)$ From Wave Models Compared to Measurements at Buoys 44008 and 44013 for the Three Storms, for Root Mean Square Error (RMS), Bias, Correlation Coefficient (R), and Scatter Index (SI)

Model	Buoy 44013				Buoy 44008				No.
	RMS (m)	Bias (m)	R	SI (%)	RMS (m)	Bias (m)	R	SI (%)	
2005 Nor'easter storm									
WW3-ST1	0.46	-0.40	0.99	19	0.85	-0.77	0.97	26	97
WWM-ST1	0.33	-0.16	0.98	14	0.92	-0.76	0.97	28	97
SWAVE	0.31	+0.08	0.99	13	0.64	-0.11	0.90	20	97
WW3-ST4	0.51	-0.40	0.98	22	0.71	-0.61	0.97	22	97
WWM-ST4	0.41	+0.20	0.98	17	0.36	+0.06	0.97	11	97
WW3-ST4m	0.35	-0.14	0.98	15	0.46	-0.26	0.97	14	97
2007 Patriot's Day Storm									
WW3-ST1	1.00	-0.86	0.93	26	1.07	-0.85	0.90	25	118
WWM-ST1	0.92	-0.75	0.87	21	1.08	-0.78	0.88	23	118
SWAVE	0.73	-0.52	0.94	19	0.62	-0.32	0.92	14	118
WW3-ST4	0.98	-0.79	0.93	25	0.78	-0.50	0.94	18	118
WWM-ST4	0.58	-0.23	0.87	13	0.62	+0.38	0.94	13	118
WW3-ST4m	0.68	-0.42	0.93	17	0.51	-0.01	0.94	12	118
2010 Boxing Day Storm									
WW3-ST1	0.70	-0.33	0.96	23	1.72	-1.32	0.88	36	70
WWM-ST1	0.83	-0.26	0.92	27	1.45	-0.89	0.87	30	70
SWAVE	0.80	+0.24	0.93	26	0.92	+0.24	0.95	19	70
WW3-ST4	0.91	-0.59	0.97	30	1.70	-1.33	0.89	35	70
WWM-ST4	0.80	-0.07	0.92	26	1.16	-0.38	0.90	24	70
WW3-ST4m	0.64	-0.30	0.97	21	1.30	-0.88	0.91	27	70

Note. In each case, the number of observations is indicated (No.).

Table 2
 Statistics for $H_s(m)$ From Wave Models Compared to Measurements at all Buoys Available at the Time of the Study, for the Three Storms, for Root Mean Square Error (RMS), Bias, Correlation Coefficient (R), and Scatter Index (SI)

Model	RMS (m)	Bias (m)	R	SI (%)	No.
2005 Nor'easter Storm					
WW3-ST1	0.62	-0.46	0.93	31	1940
WWM-ST1	0.73	-0.56	0.98	23	291
SWAVE	0.48	+0.19	0.92	39	1649
WW3-ST4	0.54	-0.36	0.93	27	1940
WWM-ST4	0.51	+0.25	0.91	33	1940
WW3-ST4m	0.44	-0.12	0.93	24	1940
2007 Patriot's Day Storm					
WW3-ST1	0.77	-0.47	0.90	26	2714
WWM-ST1	0.93	-0.62	0.85	21	354
SWAVE	0.79	+0.11	0.92	37	2478
WW3-ST4	0.72	-0.41	0.91	24	2714
WWM-ST4	0.77	+0.39	0.89	27	2714
WW3-ST4m	0.60	-0.04	0.91	20	2714
2010 Boxing Day Storm					
WW3-ST1	0.91	-0.57	0.93	29	840
WWM-ST1	1.08	-0.25	0.88	33	210
SWAVE	1.07	+0.69	0.94	37	630
WW3-ST4	0.99	-0.69	0.92	31	840
WWM-ST4	1.05	-0.01	0.90	27	840
WW3-ST4m	0.77	-0.41	0.93	25	840

Note. In each case, the number of observations is indicated (No.).

Massachusetts and buoy 44008, southeast from Nantucket by about 100 km, near the main storm track region. Corresponding scatter plots are shown in Figure 8 and summarized in the statistics in Table 1, in terms of root mean square error (RMS), bias, correlation coefficients, and scatter index (SI). Statistics for additional buoys along the North-west Atlantic coast, located in Figure 3, are given in Table 2.

4.1.1. Comparisons of Model Systems With the Same Physics (Different Numerics)

We first consider comparisons of model wave systems with the same physics. For ST1 physics, these are results for SWAVE, WW3-ST1, and WWM-ST1. As noted in the Introduction, a third-order upwind propagation scheme is used in WW3 (Tolman and WAVEWATCH IIIR Development Group 2014), lowerorder propagation schemes are used in WWM (Roland et al., 2012), and a second-order upwind scheme is used in SWAVE (Qi et al., 2009). In addition, SWAN and SWAVE use Collins (1972) formulation for the bottom friction term S_{bf} , whereas WW3 and WWM use a JONSWAP-type term which may contribute to differences in model results at buoys near the coast in shallow water. However, the simulations from these models are generally consistent with the observed results at the buoys, for the three storms, for their growth and development phases, storm peaks, and decay phases.

For the Nor'easter Storm, the simulations capture much of the peak storm values for H_s , as shown for the single and double-peaked time series for H_s at buoys 44013 and 44008 in the time series in Figure 7, the scatter plots in Figure 8, and statistics in Table 1. Among the three wave simulations using ST1 physics, SWAVE achieves the best overall

performance, followed by WWM-ST1 and WW3-ST1 with similar performances. These results are confirmed by the larger set of available buoys as reported in Table 2. In the SWAVE results, the positive bias is notable in the scatterplot in Figure 8, compared to the negative bias of the other two models, which is also apparent in results for the other two storms.

Similar results are obtained for the Patriot's Day Storm in 2007. Once again, the simulations capture much of the peak values for H_s , shown in the double-peaks in Figure 7. In this case, the negative bias of the peak H_s values is notable, shown in Figures 7 and 8 and indicated by statistical indices in Table 1. As noted in Figure 5, the modeled (WRF) winds fail to capture the dominant shape, intensity, and direction of the storm at its peak, which are suggested by the area distributions of the CFSR and NARR winds. However, a known drawback to reanalysis winds is that they tend to overestimate the spatial scale of extratropical storms because of their coarse spatial scales as suggested in Figure 5, whereas modeled winds are more accurate than reanalysis winds, particularly at observation locations like buoy 44029, shown in Figure 4. Biases in the winds result in biases in waves. Additional reasons that might account for the tendency for wave models to miss the peak sea states are given by Cavaleri (2009). Again, SWAVE is able to make the best simulation of the storm, followed by WWM-ST1 and WW3-ST1. However, although results from the larger set of buoys in Table 2 confirm that the best performance is given by SWAVE, they also suggest that WW3-ST1 outperforms WWM-ST1.

Results for the Boxing Day Storm are less unequivocal. SWAVE has the best performance at buoy 44008, followed by WWM-ST1 and WW3-ST1, which have significant negative biases, evident in Figure 8. Results at buoy 44013 suggest similar model ability for the three models. When the larger set of buoys is considered, statistical results in Table 2 suggest that WWM-ST1 and WW3-ST1 appear to slightly outperform SWAVE.

A second set of model wave systems with the same physics is WWM-ST4 and WW3-ST4 which use ST4 physics. Results are given for H_s time series in Figure 7, scatter plots in Figure 8 and statistics in Tables 1 and 2. The default values for parameters in the ST4 physics package from Ardhuin et al. (2010) are for BETAMAX, the wind-wave growth parameter, and ZALP, the wave age shift of the long waves to account for gustiness; these are set to default values optimized for the global ocean, 1.52 and 0.006, respectively, in these simulations.

In terms of capturing the peak H_s values at buoys 44013 and 44008 as given in Figures 7 and 8 and the statistical indices in Table 1, WWM-ST4 outperforms WW3-ST4 for the three storm cases. The exception is that WW3-ST4 has slightly better correlation coefficients (R) at buoy 44013 for the Patriot's Day Storm and the Boxing Day Storm. However, consideration of the larger set of buoys gives statistical results in Table 2 that suggest that the performances of the two models are essentially about the same.

4.1.2. Comparisons of Specific Models With Different Physics

We first consider WW3 and compare results from WW3 using ST1 compared to ST4. Here, the results of the comparison are not clear. In terms of capturing storm peak values and model biases, H_s time series in Figures 7 and scatterplots in Figure 8 appear to suggest similar behaviors for WW3-ST1 and WW3-ST4. Statistical indices in Table 1 also reflect the ambiguity seen in Figures 7 and 8, with WW3-ST1 outperforming WW3-ST4 at buoy 44013 for the Nor'easter Storm and the Boxing Day Storm, and the other way around, with WW3-ST4 outperforming (or similar to) WW3-ST1 for the results at buoy 44008 for the three storms, and at buoy 44013 for the Patriot's Day Storm. This trend continues in reporting statistical indices in Table 2 for the larger set of buoys; WW3-ST4 is able to outperform WW3-ST1 for the Nor'easter Storm and the Patriot's Day Storm, but not for the Boxing Day Storm.

As a second comparison, we first consider WWM and compare WWM-ST1 to WWM-ST4. The results at buoys 44013 and 44008 in Figures 7 and 8, and Table 1 suggest that the best performances are given by WWM-ST4. This is particularly evident in the model simulations of the spectral peaks of the three storm cases. Thus, ST1 physics tends to lead to underestimates which are mitigated by ST4 physics, resulting in improved RMS error values, reduced bias, and improved correlation coefficients (R) and scatter indices. These trends are particularly evident in the larger set of buoys used in Table 2. It is apparent that ST4 physics does improve the performance of WWM, compared to ST1 physics.

As an additional comparison of the ST1 and ST4 physics for a given model, we compare H_s results from WWM-ST1 and WWM-ST4 to remotely sensed altimeter H_s measurements from Jason-2 in scatter-plots in Figure 9. An example of the satellite trajectory tracks is shown in Figure 6. In these along-track comparisons,

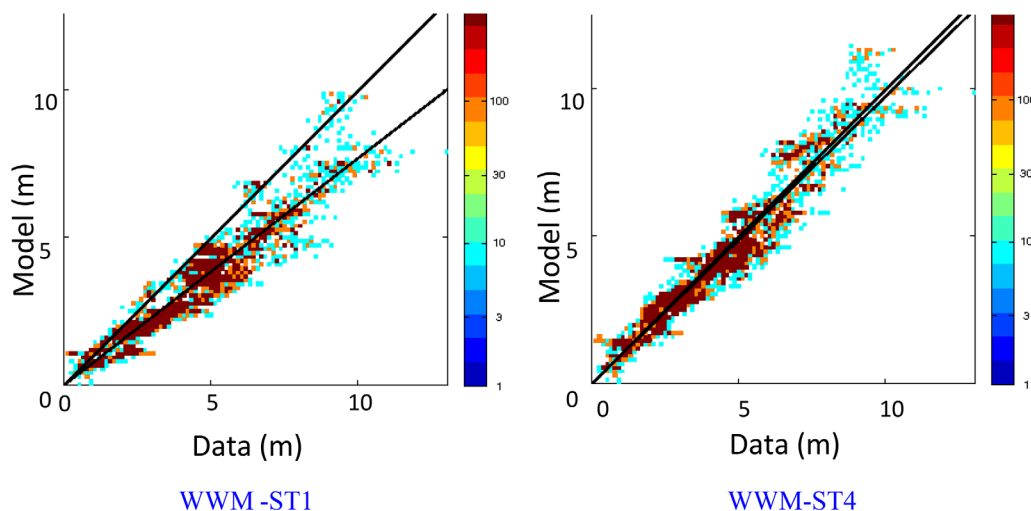


Figure 9. Comparison of H_s from WWM-ST1 and WWM-ST4 to collocated altimeter measurements of H_s from Jason-2, along the satellite trajectory and spatially described in Figure 6. Correlation coefficients are 0.94 and 0.96 for WWM-ST1 (left column) and WWM-ST4 (right column), respectively. Color bar indicates the number of points used in the comparisons.

the results from WWM-ST1 are negatively biased compared to the observed values for H_s , whereas results from WWM-ST4 have reduced scatter and negligible bias. Clearly the results of WWM-ST4 outperform those of WWM-ST1. Correlation coefficients are similar: 0.94 for WW3-ST1, compared to 0.96 for WW3-ST4.

4.1.3. Impacts of Model Tuning

We compare the results from WW3-ST4 to those from WW3-ST4m. Here, ST4m (denoting ST4 “modified”) uses adjustments to parameters BETAMAX, the wind-wave growth parameter, and ZALP, the wave age shift of the long waves to account for gustiness, respectively, 1.75 and 0.008, to give optimal simulation skill for the Northwest Atlantic and Gulf of Maine for the storms considered here.

For the two buoys, 44013 and 44008, results in Figures 7 and 8 show that this tuning of two parameters gives better performance for WW3-ST4m compared WW3-ST4, for the three storm cases, as shown by all the statistical indices on Table 1. Moreover, consideration of the larger set of buoys in Table 2 gives the same result; for all statistical indices shown, tuning of these two parameters gives better performance for WW3-ST4m than for WW3-ST4, for the three storms. However, although WW3-ST4m appears better able to capture the peak H_s values in the time series shown in Figure 7, it is apparent in Figure 8, and Tables 1 and 2, that significant bias can still occur, for example in the simulation results of the Boxing Day Storm.

It is also interesting to compare results from WW3-ST4m to those from WWM-ST4, which had no specific regional tuning of the physics parameters. Performance of these two model systems appear to be similar. In the Nor’easter Storm and the Boxing Day Storm, for the two buoys, WW3-ST4m gives better results at buoy 44013, whereas WWM-ST4 is better at buoy 44008. In the Patriot’s Day Storm, it is the other way around, with WWM-ST4 better than WW3-ST4m at 44013 and WW3-ST4m better at 44008. But consideration of the larger set of buoys in Table 2 suggests that the performance of WW3-ST4m is better than that of WWM-ST4, for almost all the statistical indices used in this study. The exception is the negative bias that is still evident in WWS-ST4m results in the Boxing Day Storm in the Figure 8 scatter plots and Table 1 statistics.

4.1.4. Biases in the Winds

In the Nor’easter Storm, all models tend to exhibit negative bias at the second peak of the H_s time series in Figure 7. This suggests a negative bias in the structure of the wind fields in this area, which can be seen by comparisons between the modeled winds and analysis winds available from NARR or the COAMPS operational model runs (NPS Monterey <http://www.usgodae.org/ftp/outgoing/fnmoc/models/coamps/>).

Unlike the other two storms, the wave models lag the development of the Boxing Day storm at both buoys by several hours, which appears to reflect a lag in the development of the wind fields, compared to the observed data. Comparisons of this section, e.g., for numerics (same physics, different model systems), or

for different model physics, or for tuning are not able to mitigate the lag effects due to biases in the wind fields. In terms of the rate of decay of model estimates for H_s as the storm passes and wave heights decrease, results again suggest that simulated H_s results do not decay as quickly as the measured H_s values, particularly SWAVE, and WWM-ST4, for example, 27 December at 12UTC ~ 28 December at buoy 44013. The lag in the modeled winds, e.g., with respect to CFSR, leads to a bias in the simulated waves.

4.2. 1-D Wave Spectra

Comparisons between 1-D (1-dimensional) wave spectra at the peak of the buoy measurements are shown in Figure 10 for the three storms. Two examples are given near the storm peaks for each of the three storms. The simulated 1-D spectra are all single-peaked. Moreover, all simulations of 1-D spectra in Figure 10 underestimate the observed values. Some of the comparisons show large discrepancies between the model simulations and observed data in Figure 10. It is also clear from the wind data in Figures 4 and 5 that wind directions do change and therefore interactions between swell and wind-waves are present during these storms.

4.2.1. Comparisons of Model Systems With the Same Physics (Different Numerics)

We first consider comparisons of model wave systems with ST1 physics, for results from WW3-ST1 and WWM-ST1 in comparison with SWAVE. In most of the examples shown, the results from WWM-ST1 achieve estimates that are closer to the observed 1-D spectra, than those given by WW3-ST1. An exception is the comparison for buoy 44008 during the Nor'easter Storm, when the WW3-ST1 results are slightly better than those from WWM-ST1. However, in all cases, the results from WW3-ST1 and WWM-ST1 are among the poorest, in terms of simulating the observed 1-D wave spectra. Results from SWAVE, also using ST1, are usually better than those of WW3-ST1 and WWM-ST1, and at 21UTC on 7 May 2005 in the Nor'easter Storm and at 12 UTC on 16 April 2007 Patriot's Day Storm, achieve the best simulations.

As a second comparison with the same physics, we consider results from WWM-ST4 and WW3-ST4 which use ST4 physics. Results shown in Figure 10 are clear. In each storm case, WWM-ST4 results exceed those of WW3-ST4, and also achieve all the best comparisons with the observed 1-D spectra data, with the exception of the SWAVE performance at 12 UTC on 16 April 2007 during the Patriot's Day Storm.

4.2.2. Comparisons of Specific Models With Different Physics

We consider WWM and compare WWM-ST1 to WWM-ST4. Again, the results shown in Figure 10 are clear. In each case, WWM-ST4 results exceed those of WWM-ST1, and achieve enhanced simulation of the observed 1-D spectral data. As a second comparison we focus on results from WW3-ST1 and WW3-ST4. Here, again the results are unequivocal, as for WWM. In each case, WW3-ST4 results outperform those from WW3-ST1, and give better simulations of the observed 1-D spectral data.

4.2.3. Impacts of Model Tuning

The results from WW3-ST4 are compared to those of WW3-ST4m, both using ST4 physics; here, ST4m uses two adjusted physics parameters (BETAMAX and ZALP) to give optimal simulation skill for the Northwest Atlantic and Gulf of Maine for the storms considered in this study. Here again, the results are clear. In each case, results from WW3-ST4m outperform those from WW3-ST4, in terms of comparisons with the observed 1-D spectra at the buoys.

4.3. 2-D Wave Spectra

Comparisons between 2-D measured data and model simulations (using ST4 physics) for the Boxing Day storm at its peak (15UTC and 18UTC on 27 December) are shown in Figure 11 for buoy 44008. The buoy results are calculated following the Longuet-Higgins approximation for the Fourier expansion method as recommended by the NDBC website (www.ndbc.noaa.gov/measdes.shtml). The observed data in Figure 11a show the response of the wave spectra to turning winds, as the primary peak shifts to a secondary peak at 18UTC. Model simulations at 18 UTC suggest qualitatively similar results. Although the main directions for the two peaks approximately match the observed peaks, the modeled maximum energy values are over-estimated, compared to the observations, with values, 53.5 m^2/Hz at 15 UTC and 26.8 Hz at 18UTC. The models also exhibit differences with observed data in terms of the extent to which wave energy has been generated in the new developing wind direction.

4.3.1. Comparisons of Model Systems With the Same Physics (Different Numerics)

We consider results from WWM-ST4 and WW3-ST4 which use ST4 physics. As shown in Figure 11b, WWM-ST4 puts more energy in the direction of the new developing spectral peak by 18 UTC at $\sim 105^\circ$, with less energy in the direction of the original peak, at $\sim 15^\circ$. The transition to the new wind direction is *similar* to the

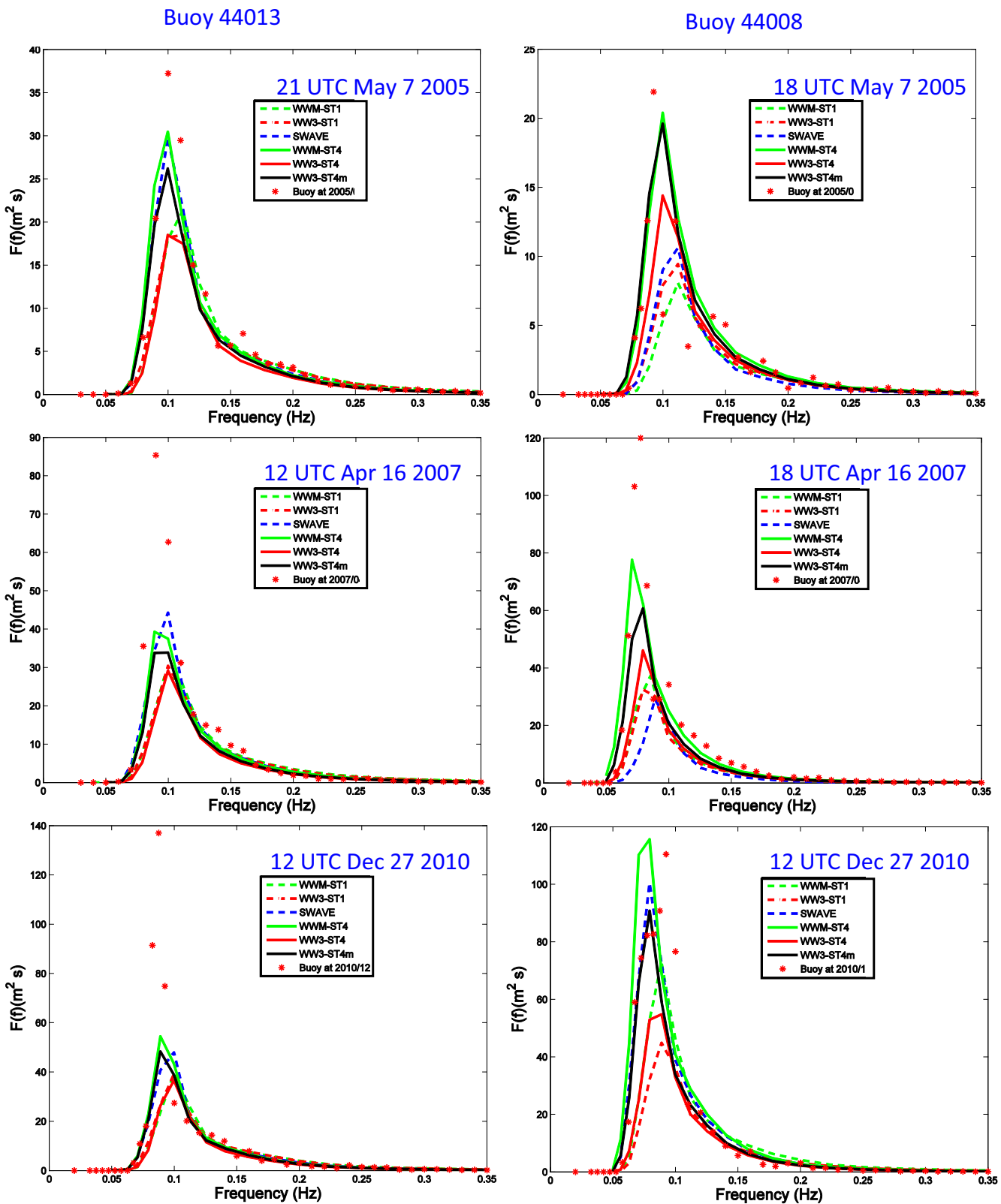


Figure 10. One-dimensional energy spectra, plotting energy spectra versus frequency, f , in comparison with observations from buoys 44013 (left side) and 44008 (right side), at the peak observed storm in each of three cases: (top row) 2005, (middle) 2007, and (bottom) 2010. Model configurations are indicated.

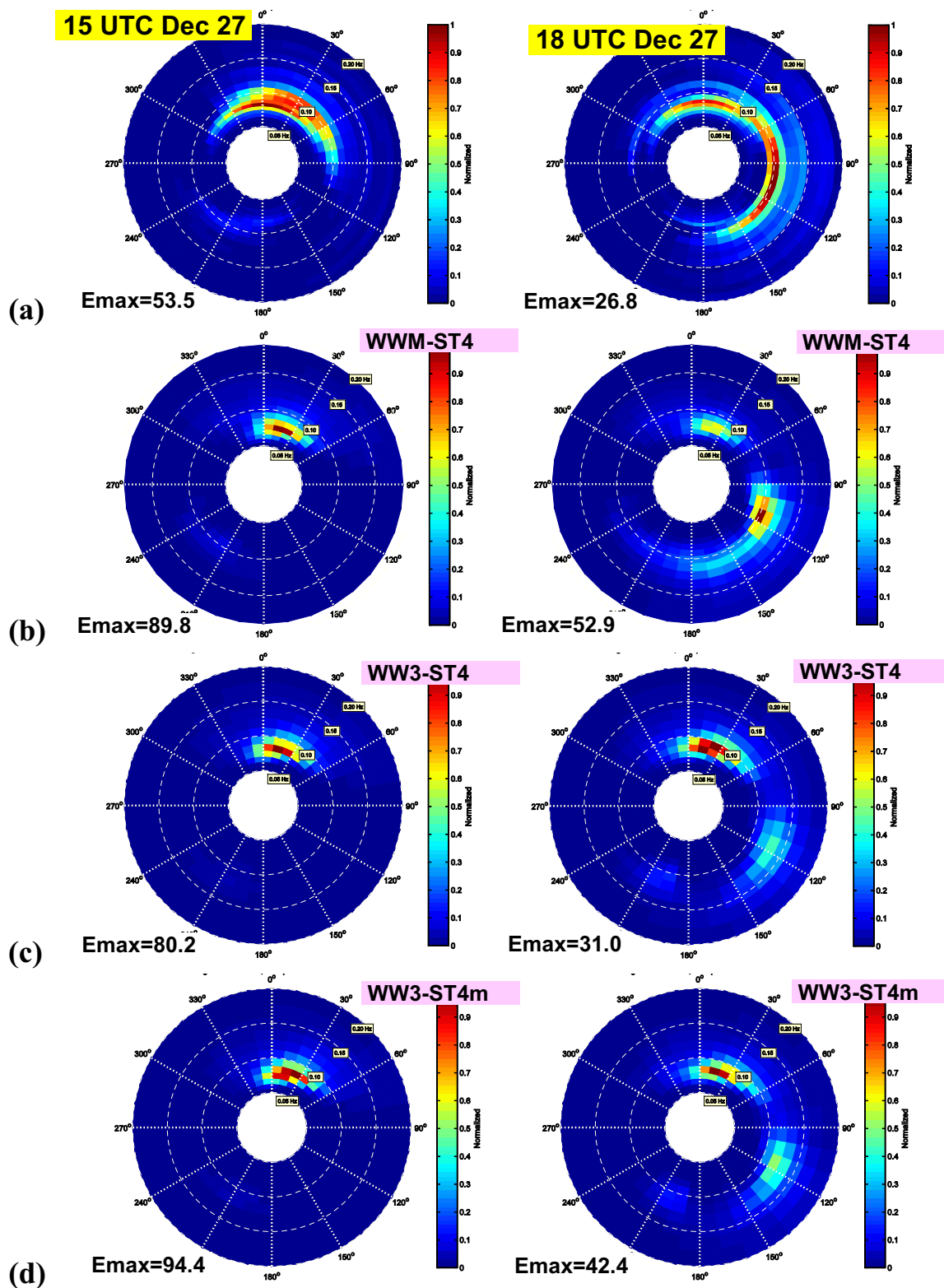


Figure 11. Comparisons of 2-D spectra for the 2010 Boxing Day Storm at the peak (15UTC and 18UTC on 27 December) shown in Figure 7 at buoy 44008: (a) observed 2-D spectra (top row), (b) model spectra from WWM-ST4 (second from top), (c) from WW3-ST4 (third from top), and (d) from WW3-ST4m (bottom). The spectra are normalized by the maximum in each plot. Frequency increments are 0.05 Hz. Comparisons of 2-D spectra for the 2010 Boxing Day Storm after the peak (15UTC on 28 December): (e) observed 2-D buoy spectra, (f) model spectra from WWM-ST4m, and (g) from ENVISAT synthetic aperture radar (SAR) at 14:43 UTC at location indicated . The spectra are normalized by the maximum in each plot. The buoy 44008 location is indicated .

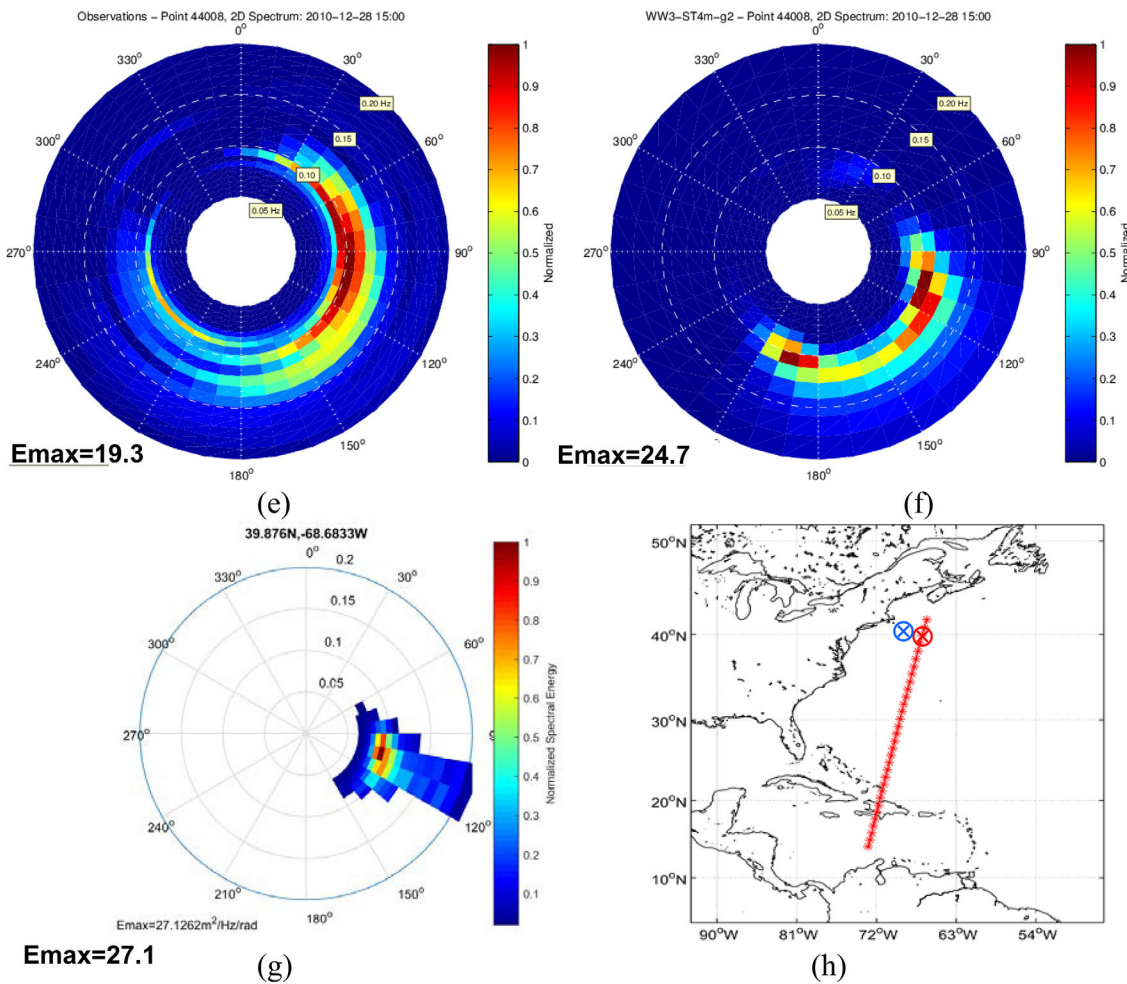


Figure 11. (Continued).

transition observed in the buoy data. Compared to WWM-ST4 and the buoy observations, the WW3-ST4 simulation appears to be slower in responding to the wind direction shift shown in Figure 4; less energy is put in the direction of the *new* developing peak, compared to the original peak. Moreover, it is also apparent that these model results are both too high, with maximum energy at 52.9 m²/Hz for WWM-ST4 results, whereas results from WW3-ST4 are more moderate with maximum energy values of 31.0 m²/Hz, more consistent with the observed maximum buoy energy, but in the direction of the original peak at 15 UTC. Thus, relatively less energy has been passed to the direction of the new developing peak by WW3-ST4 by 18 UTC. These results reflect bias in the directional shifting of the WW3-ST4 modeled results, in response to the veering winds, compared to WWM. Thus, the only model features that differentiate WWM-ST4 from WW3-ST4 are the unstructured and structured grids, respectively, and the propagation numerics which also relates to time-stepping. Although the DIA (discrete interaction approximation) parameterization for the nonlinear wave-wave interactions (S_{nl}) has a role in transferring energy to changing directions, driven by wind changes, the formulation is the same in both models, and therefore DIA cannot explain the differences shown in Figure 11 at 18 UTC.

4.3.2. Impacts of Model Tuning

The results from WW3-ST4 are not significantly different from those of WW3-ST4m, except in terms of the magnitude of the simulated 2-D spectral peaks, compared to the observed data. Both use ST4 physics. Figure 11 suggests that although tuning of the two parameters, BETAMAX, the wind-wave growth parameter and ZALP, the wave age shift of the long waves to account for gustiness may improve simulations of H_s in Table 2 and in the 1-D spectra in Figure 10 that is not the case for the 2-D spectra. It appears that tuning favors enhancement of the main spectral peaks and is not able to address the model's respond to shifting

winds. Moreover, as the formulation for the nonlinear wave-wave interactions, S_{nl} , is given by the DIA formulation in all the models used in this study, tuning cannot change the results.

Another possibly essential difference between WWM-ST4 and WW3-ST4 or WW3-ST4m is numerics, in terms of the shifting direction of the spectral peak, with third-order upwind propagation in WW3 and lower-order propagation schemes in WWM. This is the mechanism that can determine the rapidity with which the model shifts the dominant direction of the wave spectral in response to a shifting wind direction. But in the results shown in Figure 11, numerics are not able to make notable differences in terms of the wave models' inability to respond to veering wind directions.

4.3.3. Completion of the Turning Event

A few hours later, at 15:00UTC on 28 December, the turning event is essentially complete, and the winds are relatively constant, as indicated in Figure 4. It is interesting to compare model estimates from WW3-ST4m to buoy and satellite data. At this time, 2-D wave spectra are available from synthetic aperture radar (SAR) onboard ENVISAT, along the satellite track shown in Figure 11h. The SAR image is located at (39.876°N 68.683°W) as shown in Figure 11h, whereas the buoy is rather distant, 1.94° ~216 km away, at (40.504°N 69.248°W). The retrieved SAR data at 14:43 UTC shows a peaked spectrum in Figure 11g with maximum energy 27.1 m²/Hz, which corresponds reasonably well to the maximum suggested by the buoy. As shown in Figure 11e, the latter is smoothed, characteristic of the retrieval process for the Longuet-Higgins method. The directions of the spectral peaks are approximately consistent, although SAR spectrum appears to turn more than the buoy spectrum, perhaps indicative of the distance between the two measurements. Results from the simulation by WW3-ST4m, at the location of the buoy, are shown in Figure 11f. The maximum energy from the model is 24.7 m²/Hz, which is consistent with buoy measurements. The peak direction is also consistent with the peak direction indicated by the buoy, at about 125°. The model results also indicate a secondary peak at 200°, which is also suggested by the buoy measurements, but not evident in the SAR imagery. However, like buoy observations, SAR imagery has limitations in terms of resolution of the directional wave spectra (Xie et al., 2015; Zhang et al., 2010).

4.4. 2-D Maximum H_s Distributions

This section explores the shape and intensity of the maximum H_s field at the peaks of the storms, as produced by a selection of the wave model simulations. We consider WW3-ST4m because two of the physical parameters were adjusted to reflect the characteristics of ocean waves in the Northwest Atlantic, WWM-ST4, because it is an unstructured grid version of WW3 using ST4 physics, and SWAVE, because it is an unstructured grid model using ST1.

Comparisons of the spatial distributions of significant height fields H_s near the peaks of the three storms are shown in Figure 12 for WW3-ST4m, WWM-ST4, and SWAVE, showing the main area of each storm. The SWAVE domain is smaller than those of the other two models (as indicated in Figure 2) and cannot really represent the entire area of these storms with the area of its regional grid, because SWAVE relies on nesting within a larger regular grid where WW3 is implemented at resolution about ~10 km (Chen et al., 2013), indicated in Figure 2b. However, SWAVE is still shown to perform well in comparisons with larger buoy sets, as discussed in section 4.

The results shown for the three storms, for WW3-ST4m and WWM-ST4 indicate the spatial scale of these storms, from coastal areas of Nova Scotia to waters off Cape Hatteras with an east-west cross-section of the order of 2,000 km extending into the northwest Atlantic. For the Nor'easter Storm, maximum H_s wave heights reach more than 7 m from WW3-ST4m, and slightly less in results from WWM-ST4. Similar results are obtained in the Patriot's Day storm, with maximum storm intensity of about 9 m from WW3-ST4m, and reduced maximum storm intensity in results from WWM-ST4. Results from the Boxing Day storm are similar to those of the previous two storm cases, with a similar large spatial extent as suggested by the H_s distributions from WW3-ST4m, and WWM-ST4, and maximum H_s values of about 10 m from WW3-ST4m.

Due to differences among wave model simulations such as tuning in WW3-ST4m, in modifying the physics parameters for wind-wave coupling and the wave age shift to account for gustiness, certain portions of the wave field are scaled up compared to WWM-ST4. As shown in Figure 12, this tends to occur in the forward right quadrant of the storm, the area where winds tend to be the highest. For example, the Boxing Day Storm exhibits a prominent vortex-like pattern in the H_s distribution, south of Long Island and the Rhode

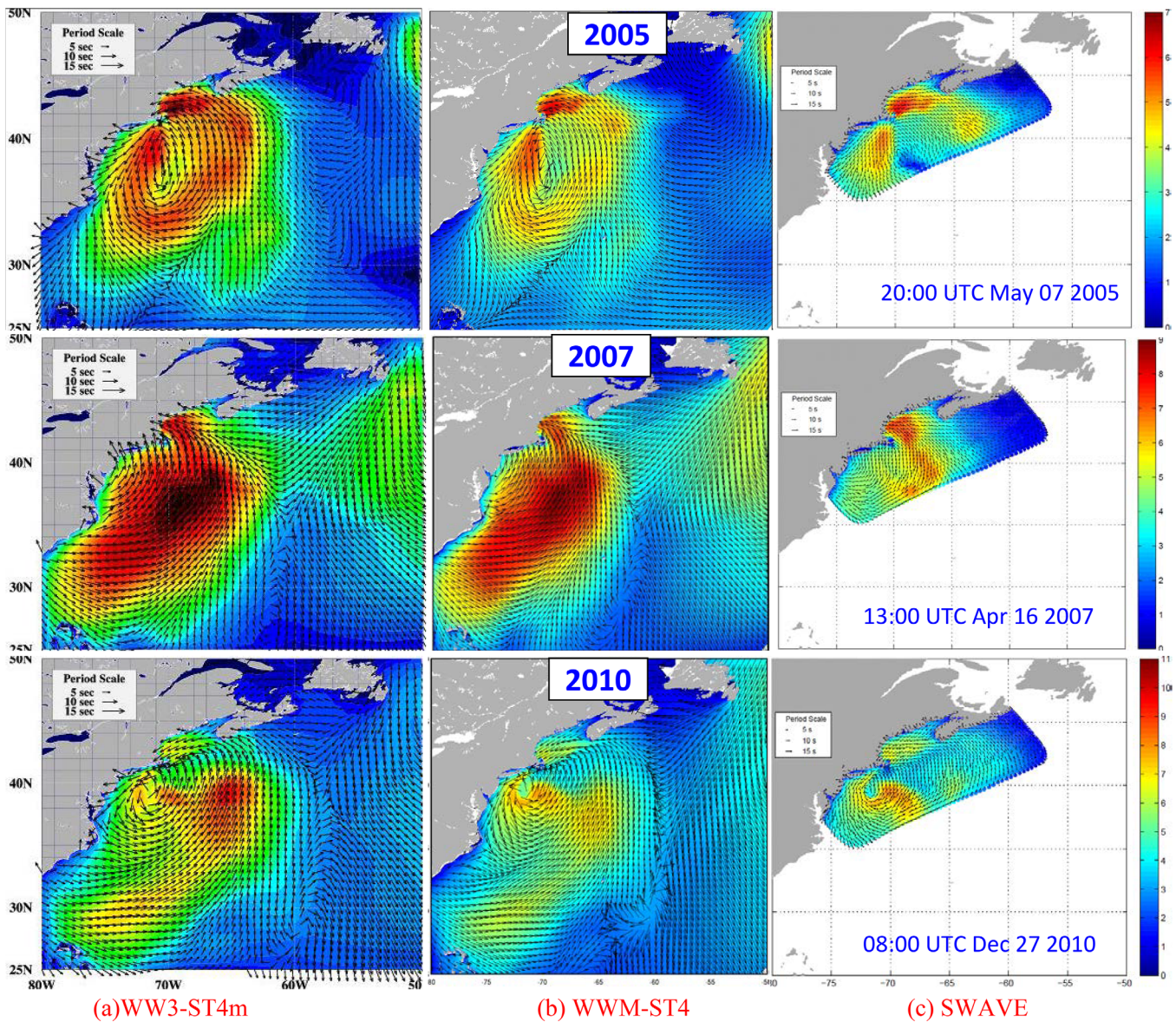


Figure 12. Maps for H_s near the peak of each storm from (left column) WW3-ST4m, (middle column) WWM-ST4m, and (right column) SWAVE, for the (top row) 2005 Nor'easter Storm, (middle) 2007 Patriot's Day Storm, and (bottom) 2010 Boxing Day Storm.

Island coast; with an eastern "tail" that is not as evident in results from WWM-ST4 as in those from WW3-ST4m.

4.5. H_s Swath Distributions

An additional exploration of the overall shape and intensity of the maximum H_s field at the peaks of the storms can be displayed as composite results in H_s swath plots, which give the maximum H_s at every grid point during the passage of a storm. Figure 13 displays results for models using ST4 physics. Results for H_s swath plots produced by WW3-ST4, WW3-ST4m, and WWM-ST4 are presented. As in the presentation of maximum H_s results, a large domain grid is shown to give an overview of the spatial variations within the H_s swath distribution. While the H_s swath plots have some similarity to the maximum H_s plots in Figure 12, they provide additional characteristics.

In terms of comparisons of model systems with the same physics (different numerics), we first compare results from WW3-ST4 and WWM-ST4. The overall structures of the three storms are similar in the regions of maximum storm intensity. The H_s swath simulations from WWM-ST4 are slightly more intense than those

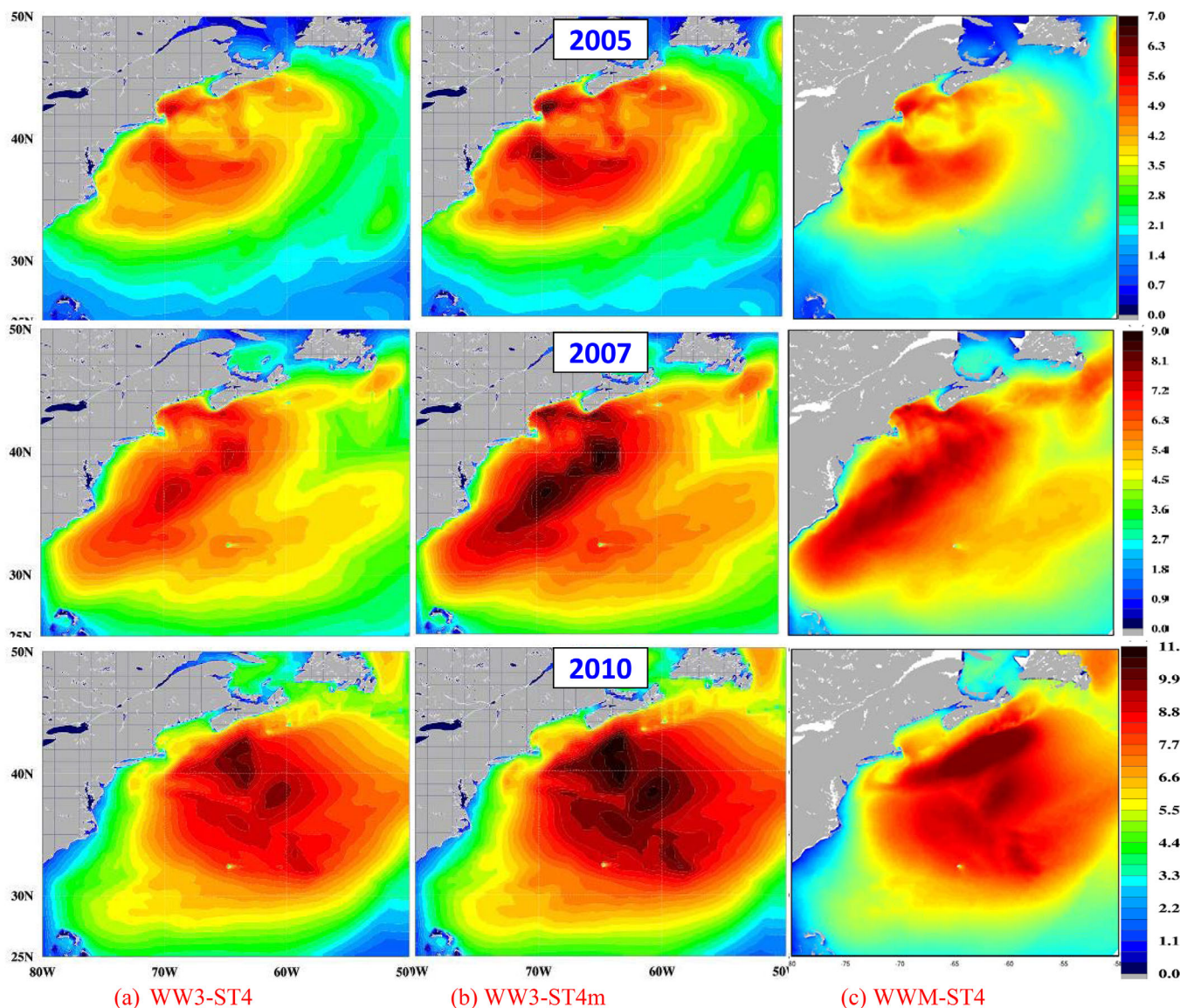


Figure 13. Swath maps for H_s (m), showing maximum H_s at every grid point of the integration domain, during the passage of the storms from (left column) WW3-ST4, (middle column) WW3-ST4m, and (right column) WWM-ST4, for the (top row) 2005 Nor'easter Storm, (middle row) 2007 Patriot's Day Storm, and (bottom row) 2010 Boxing Day Storm.

generated by WW3-ST4, consistent with earlier results shown in Figure 10 for 1-D spectra near the storm peaks. The swath plots allow the assessment that for the Patriot's Day Storm this feature is an elongation of the high H_s band from southwest to northeast, for both WW3-ST4 and WWM-ST4. By comparison, the results for the other two storms are more "bunched" and less of an elongation, for all three models considered in Figure 13.

In terms of the impacts of model tuning, H_s results from WW3-ST4m generally appear to be similar to those resulting from WW3-ST4, except that the H_s swath values are larger for the three storms. In the tuning that is done in WW3-ST4m, it is apparent that, with the passage of the storms, the H_s swath plots have increased values for essentially all portions of the WW3-ST4m wave field, for the overall swath results, compared to WW3-ST4.

5. Discussion

Based on the comparisons among model results, we find the following results.

5.1. Comparisons of Model Systems With the Same Physics (Different Numerics)

In terms of time series of significant wave heights H_s at specific buoys for the three storm cases, the three wave model systems are able to provide simulations that are in reasonable agreement with storm-generated values for H_s as measured at the buoys. In terms of *ST1 physics*, among the three wave simulations using *ST1 physics*, SWAVE achieves the best overall performance, followed by WWM-ST1 and WW3-ST1 with similar performances. By comparison, for *ST4 physics*, the overall performances of WWM-ST4 and WW3-ST4 for the set of available buoys are essentially similar; although WWM-ST4 outperforms WW3-ST4 for just the two buoys 44013 and 44008 on the relatively small local scale of the Massachusetts coastal area of the southern Gulf of Maine.

We also computed the areal distributions of maximum H_s and also H_s swath plots for the three storms. These indicate that for *ST4 physics*, results from WWM-ST4 compared to WW3-ST4 and WW3-ST4m, are intermediate in terms of H_s values, resulting from the unstructured grid and the numerics that are used in the latter, which also suggest some elongation of the H_s max plots, particularly for the Patriot's Day Storm. By comparison, tuning in WW3-ST4m, results in overall increased H_s values in the swath plots.

In terms of *1-D wave spectra*, all simulations of 1-D spectra underestimate the observed values. While WWM-ST1 achieves estimates that are closer to the observed 1-D spectra than those given by WW3-ST1, both WW3-ST1 and WWM-ST1 are among the poorest of the wave simulations. By comparison, results from SWAVE, also using *ST1*, are usually much better than those of WW3-ST1 and WWM-ST1, and sometimes achieve the best simulation for specific buoy cases. By comparison, 1-D wave spectra results from WWM-ST4 always outperform those of WW3-ST4.

In terms of *2-D wave spectra*, measured data were limited to a turning wind test case for just the Boxing Day Storm at buoy 44008. Although results are presented for model systems using *ST4 physics*, all respond too slowly compared to the observed directional wind shift data. We suggest that this situation may occur because of the formulation for the nonlinear wave-wave interactions (S_{nl}) that each model uses. Additional studies of the wave response to veering winds are being pursued in a separate study that focuses on S_{nl} .

5.2. Comparisons of Specific Models With Different Physics

In terms of H_s , for the three storm cases for WW3-ST1 and WW3-ST4, results from *ST4 physics* are slightly better than those from *ST1 physics*, in comparisons with measurements from the buoys 44013 and 44008 near the southern Gulf of Maine, as well as the statistical indices reported for the larger set of buoys in Table 2. Moreover, similar comparisons clearly reveal that WWM-ST4 outperforms WWM-ST1, as particularly evident in statistical indices from comparisons with buoy data. In terms of 1-D wave spectra for the three storm cases, results indicate that WWM-ST4 outperforms WWM-ST1 and WW3-ST4 outperforms WW3-ST1.

5.3. Impacts of Model Tuning

In terms of H_s , the results from the three storm cases suggest that WW3-ST4m outperforms WW3-ST4, which is not a surprise, for all the statistical indices. Moreover, in comparisons with buoy measurements near the southern Gulf of Maine, WW3-ST4m has similar model skill to that of WWM-ST4, whereas for the larger set of buoys, the performance of WW3-ST4m is better than that of WWM-ST4. In terms of 1-D wave spectra for the three storm cases, the results from WW3-ST4m outperform those from WW3-ST4. However, for 2-D wave spectra, tuning cannot improve the model response of WW3-ST4m to veering wind directions.

6. Conclusions

We compared three wave model systems: (a) a *structured* grid model system with SWAN implemented on nested high-resolution grids, within coarser grids where WW3 is implemented, (b) SWAN implemented on nested finite-volume *unstructured* grid domains, denoted SWAVE, and (c) WWM implemented on a single finite-element unstructured grid. Differences in the model systems are due to differences in the numerics, the propagation schemes, the source term parameterizations for S_{in} and S_{ds} , the way the source terms (denoted *ST1*, *ST4*, and *ST4m*) have been integrated in the model systems, and the *structured* or *unstructured* grids. Three intense nor'easter cyclones were selected as test cases for intercomparisons, with common winds used for each storm simulation based on MM5 or WRF model simulations.

We first make comparisons between all *model systems with the same physics (different numerics)*. Second, we make *model comparisons of different physics* (ST1, ST4, and ST4m). Finally, we investigate the impact of *model tuning* to reflect the regional characteristics of the focus area of this study. In the first set of comparisons, between models with the same physics, we want to see how results differ by using different numerics. In the second set of comparisons, we want to emphasize the need for improved more complete physics, in forecast model systems.

SWAN, SWAVE, and WWM use lower-order propagation schemes, whereas WW3 uses higher-order schemes. All model systems use relatively simple ST1 physics for S_{in} and S_{ds} , based on the WAM cycle three parameterizations; these are indicated as WW3-ST1, WWM-ST1, and SWAVE models in the comparison tests. WW3 and WWM can also use the state-of-the-art forms for S_{in} and S_{ds} for operational forecast models (Arduin et al., 2010), denoted as WW3-ST4 and WWM-ST4, respectively. The ST4 formulation is more physically based than ST1, taking into account a more detailed description of the dynamics of wind growth and dissipation source terms. However, there is a cost for the improved results; the computational difference between the two parameterizations is at least 50% because of a number of reasons: (a) ST4 uses a broader prognostic frequency range than ST1, (b) ST4 uses a more complex wind input term S_{in} than that of ST1 including a quasi-linear parameterization proposed by Janssen (1991) and adding a sheltering term, (c) the wave breaking term contains two parts, an inherent breaking term, a cumulative term and is tuned to be anisotropic, and (d) an additional swell-decay term is included in S_{in} . In this regard, it is notable that the recently developed observation-based source term package ST6 shows close accuracy to ST4 but at less computational cost (Liu et al., 2017; Rogers et al., 2012; Zieger et al., 2015) and may therefore be of interest for future studies and tests with the three storm cases considered here.

6.1. Comparisons of Model Systems With the Same Physics (Different Numerics)

Wave model systems that use ST1 physics can capture much of the peak intensity of H_s time series generated by nor'easter-type storms. This is particularly evident in results from SWAVE. By comparison, models using ST4 physics (WWM-ST4 and WW3-ST4) have overall performances that are essentially similar, implying that the effects of the *unstructured* and *structured* grids are secondary, as are the effects of numerics in the propagation schemes for comparisons at specific buoys. Maps of maximum H_s distributions and H_s swath plots suggest that the lower-order numerics of WWM-ST4 lead to intermediate values for the H_s fields, compared to WW3-ST4 and WW3-ST4m results. In terms of 1-D wave spectra, while all wave simulations tend to underestimate the observed values, results from model simulations that use ST1 are generally quite poor, except that SWAVE results can sometimes achieve relatively good simulations for specific buoys. By comparison, models using ST4 are the best, with WWM-ST4 always outperforming WW3-ST4. In terms of 2-D wave spectra, models displayed differences in their inability to respond to veering wind directions. The best performance appears to be that of WWM-ST4. We attribute this result to the unstructured grid and the numerics that are used by this model. In addition, a suspected factor is the inadequacy of the parameterization for the nonlinear wave-wave interactions (S_{nl}) that each model uses, the DIA parameterization, but that is not clear in our present simulations. Finally, SWAN and SWAVE use Collins (1972) bottom friction whereas WW3 and WWM use a JONSWAP-type formulation which may also contribute to differences in results.

6.2. Comparisons of Specific Models With Different Physics

In terms of H_s or 1-D wave spectra, results obtained from wave model systems using ST4 physics are better than those from ST1 physics, whether based on WW3 or on WWM models. The physics implemented by ST4 is important, and should be implemented to improve the performance of models like SWAVE. Regarding propagation schemes, based on this regional study, summarized in Table 2, it is not clear that the propagation schemes implemented in the models and associated methodologies to integrate source terms give better results than higher-order propagation schemes as implemented in WW3 compared to lower-order propagation schemes implemented in SWAN, SWAVE, and WWM. Results appear to be almost the same because of the smoothing used to reduce the garden sprinkler effect.

6.3. Tuning

Tuning can improve model results. When physics parameters adjusted to global ocean applications are modified to the regional characteristics of the Northwest Atlantic and the Gulf of Maine, as applied in WW3-ST4m, wave model simulation results can be improved. Thus, enhanced H_s simulations were possible, and comparisons with the buoy measurements suggest that the performance of WW3-ST4m is the overall best, for H_s distributions as well as for comparisons of 1-D wave spectra.

Acknowledgments

This work was supported by the NOAA-funded IOOS/SURA hurricane and extratropical storm-induced inundation testbed programs grant to BIO (NA11NOS0120141). We also acknowledge support from the Canadian Panel on Energy R & D (#1B00.003C), and Fisheries and Oceans Canada's Aquatic Climate Change Adaptation Program (#MAR-9). Data sets used in the model comparisons consist of in situ observations from NDBC (National Data Buoy Center) buoys (www.ndbc.noaa.gov), satellite altimeter (Jason-1, Jason-2, ENVISAT, and ERS-2) available from ftp://ftp.aviso.altimetry.fr/pub/oceano/AVISO/wind-wave/nrt/mswh/merged/, and ENVISAT SAR wave data from http://globwave.ifremer.fr. We would like to thank the anonymous reviewers who helped improve the manuscript.

References

Arduin, F., Rogers, E., Babanin, A. V., Filipot, J. F., Magne, R., Roland, A., . . . Collard, F. (2010). Semiempirical dissipation source functions for ocean waves. Part I: Definition, calibration, and validation. *Journal of Physical Oceanography*, *40*(9), 1917–1941. <https://doi.org/10.1175/2010JPO4324.1>

Battjes, J. A., & Janssen, J. P. F. M. (1978). Energy loss and set-up due to breaking of random waves. In *Proceedings of the 16th International Conference on Coastal Engineering* (pp. 569–587). Reston, VA: American Society of Civil Engineers.

Booij, N., Ris, R. C., & Holthuijsen, L. H. (1999). A third-generation wave model for coastal regions, Part 1: Model description and validation. *Journal of Geophysical Research*, *104* (C4), 7649–7666.

Cardone, V. J., Jensen, R. E., Resio, D. T., Swail, V. R., & Cox, A. T. (1996). Evaluation of contemporary ocean wave models in rare extreme events: the Halloween Storm of October 1991 and the Storm of the Century of March 1993. *Journal of Atmospheric and Oceanic Technology*, *13*(1), 198–230.

Cavaleri, L. (2009). Wave modeling missing the peaks. *Journal of Physical Oceanography*, *39*(11), 2757–2778. <https://doi.org/10.1175/2009JPO4067.1>

Chen, C., Beardsley, R. C., Luettich, R., Westerink, J., Wang, H., Perrie, W., . . . Toulany, B. (2013). IOOS/SURA Extratropical Storm Inundation Testbed: Inter-model (ADCIRC, FVCOM and SELFE) comparisons in Scituate, Massachusetts. *Special Issue of Journal of Geophysical Research on U.S. Integrated Ocean Observing System Coastal Ocean Modeling Testbed*, *118*, 5054–5075.

Collins, J. I. (1972). Prediction of shallow water spectra. *Journal of Geophysical Research*, *77*(15), 2693–2707.

Donald Cameron and George Parkes. (1992). A meteorological overview of the Halloween Storm of 1991. In Swail, V. (Ed.), *Proceedings of the 3rd International Workshop on Wave Hindcasting and Forecasting*. Environment Canada (pp. 1–44). Toronto, Ontario, Canada: Environment Canada.

Dutour Sikirić, D., Roland, A., Tomažič, I., & Janeković, I. (2012). Hindcasting the Adriatic Sea near-surface motions with a coupled wave-current model. *Journal of Geophysical Research*, *117*, C00J36. <https://doi.org/10.1029/2012JC007950>

Grell, G. A., Dudhia, J., & Stauffer, D. R. (1995). *A description of the fifth-generation Penn State/NCAR Mesoscale Model (MM5)* (NCAR Tech. Note NCAR/TN-398 + STR 122 pp.).

Hasselmann, K. (1960). Grundgleichungen der seegangsvoraussage. *Schiffstechnik*, *7*, 191–195.

Hasselmann, K. (1962). On the nonlinear energy transfer in a gravity wave spectrum. Part 1. *Journal of Fluid Mechanics*, *12*, 481–500.

Hasselmann, K., Barnett, T., Bouws, P., Carlson, E. H., Cartwright, D., Enke, E. K., . . . Walden, H. (1973). Measurements of wind-wave growth and swell decay during the Joint North Sea Wave Project (JONSWAP). *Ergänzungsheft zur Deutschen Hydrographischen Zeitschrift, Reihe A*(8), *12*, 95 pp.

Hasselmann, S., Hasselmann, K., Allender, J. H., & Barnett, T. P. (1985). Computations and parameterizations of the nonlinear energy transfer in a gravity-wave spectrum, part II: Parameterizations of the nonlinear energy transfer for application in wave models. *Journal of Physical Oceanography*, *15*, 1378–1391.

Janssen, P. A. E. M. (1991). Quasi-linear theory of wind wave generation applied to wave forecasting. *Journal of Physical Oceanography*, *21*, 1,631–1,642.

Komen, G. J., Hasselmann, S., & Hasselmann, K. (1984). On the existence of a fully developed windsea spectrum. *Journal of Physical Oceanography*, *14*, 1271–1285.

Liu, Q., Babanin, A., Fan, Y., Zieger, S., Guan, C., & Moon, I. J. (2017). Numerical simulations of ocean surface waves under hurricane conditions: assessment of existing model performance. *Ocean Modelling*, *118*, 73–93. <https://doi.org/10.1016/j.ocemod.2017.08.005>

Mesinger, F., Dimego, G., Kalnay, E., Mitchell, K., Shafran, P. C., Ebisuzaki, W., . . . Shi, W. (2006). North American regional reanalysis. *Bulletin of the American Meteorological Society*, *87*, 343–360.

Patankar, S. V. (1980). *Numerical heat transfer and fluid flow: Computational methods in mechanics and thermal science* (p. 210). Washington, DC: Hemisphere Publishing Corporation.

Powers, J. G., Klemp, J. B., Skamarock, W. C., Davis, C. A., Dudhia, J., Gill, D. O., . . . Duda, S. E. (2017). The weather research and forecasting model: Overview, system efforts, and future directions. *Bulletin of the American Meteorological Society*, *98*, 1717–1737. <https://doi.org/10.1175/BAMS-D-15-00308.1>

Qi, J., Chen, C., Beardsley, R. C., Perrie, W., Lai, Z., & Cowles, G. (2009). An unstructured-grid finite-volume surface wave model (FVCOM-SWAVE): Implementation, validations and applications. *Ocean Modelling*, *28*, 153–166. <https://doi.org/10.1016/j.ocemod.2009.01.007>

Queffelec, P., & Croiz-Fillon, D. (2017). *Global altimeter SWH data set. User Guide, Laboratoire d'Océanographie Spatiale* (10 pp.). Paris, France: IFREMER. Retrieved from ftp://ftp.ifremer.fr/ifremer/cersat/products/swath/altimeters/waves/documentation/altimeter_wave_merge_11.4.pdf

Rogers, E. W., Babanin, A. V., & Wang, D. W. (2012). Observation-consistent input and whitecapping dissipation in a model for wind-generated surface waves: Description and simple calculations. *Journal of Atmospheric and Oceanic Technology*, *29* (9), 1329–1346. <https://doi.org/10.1175/JTECH-D-11-00092.1>

Roland, A. (2009). *Development of the WWM II - Spectral wave modelling on unstructured meshes* (PhD thesis). Darmstadt, Germany: Department of Hydraulic Engineering, University of Darmstadt.

Roland, A., Zhang, Y. J., Wang, H., Meng, V. Y., Teng, Y., Maderich, C., . . . Zanke, M. U. (2012). A fully coupled 3D wave-current interaction model on unstructured grids. *Journal of Geophysical Research*, *117*, C00J33. <https://doi.org/10.1029/2012JC007952>

Saha, S., Moorthi, S., Pan, H., Wu, X., Wang, J., Nadiga, S., . . . Goldberg, M. (2010). The NCEP climate forecast system reanalysis. *Bulletin of the American Meteorological Society*, *91*, 1015–1057.

Snyder, R. L., Dobson, F. W., Elliott, J. A., & Long, R. B. (1981). Array measurements of atmospheric pressure fluctuations above surface gravity waves. *Journal of Fluid Mechanics*, *102*, 1–59.

Tolman, H. L. (2002). *User manual and system documentation of WAVEWATCH-III version 2.22* (technical note). Camp Springs, MD: NOAA. Retrieved from http://polar.ncep.noaa.gov/waves

Tolman, H. L. (2008). A mosaic approach to wind wave modeling. *Ocean Modelling*, *25*, 35–47.

Tolman, H. L. (2009). *User manual and system documentation of WAVEWATCH III® version 3.14*. Camp Springs, MD: NOAA. Retrieved from http://polar.ncep.noaa.gov/mmab/papers/tn276/MMAB_276.pdf

Tolman, H. L., & WAVEWATCH III® Development Group. (2014). *User manual and system documentation of WAVEWATCH III® version 4.18*. College Park, MD: NOAA. Retrieved from http://polar.ncep.noaa.gov/waves/wavewatch/manual.v4.18.pdf

WAMDI Group (13 authors) (1988). The WAM model: A third generation oceans wave prediction model. *Journal of Physical Oceanography*, *18*, 1775–1810.

Xie, T., Perrie, W., He, Y. J., Li, H. Y., Fang, H., Zhao, S. Z., & Yu, W. J. (2015). Ocean surface wave measurements from fully polarimetric SAR imagery. *Science China in Earth Sciences*, *58*(10), 1849–1861. <https://doi.org/10.1007/s11430-015-5078-6>

Zhang, B., Perrie, W., & He, Y. (2010). Validation of RADARSAT-2 fully polarimetric SAR measurements of ocean surface waves. *Journal of Geophysical Research*, *115*, C06031. <https://doi.org/10.1029/2009JC005887>

Zieger, S., Babanin, A. V., Rogers, W. E., & Young, I. R. (2015). Observation-based source terms in the third-generation wave model WAVEWATCH. *Ocean Modelling*, *218*, 1–24. <https://doi.org/10.1016/j.ocemod.2015.07.014>